Measurement of lepton-identification efficiencies for searches for supersymmetry in events with two taus in the final state

Masterarbeit an der Fakultät für Physik
der

Ludwig-Maximilians-Universität München

Yasmine Israeli

München, 04.06.2014

Messung von Lepton-Identifikations-Effizienzen für Suchen nach Supersymmetrie in Ereignissen mit zwei Taus im Endzustand

Masterarbeit an der Fakultät für Physik
der

Ludwig-Maximilians-Universität München

Yasmine Israeli

München, 04.06.2014

Gutachterin: Prof. Dr. Dorothee Schaile

Abstract

The Large Hadron Collider (LHC) is the largest and most powerful collider in the world. It is designed for proton-proton and heavy-ion collisions at high energies and luminosities in order to explore the Standard Model (SM) and search for physics beyond. One of the major experiments at the LHC is the ATLAS experiment. It is a multi-purpose experiment and one of its main targets is the search for supersymmetric particles.
Supersymmetry unifies the strength of the electroweak and the strong interactions at high energies and provides a solution to the SM hierarchy problem as well as dark matter candidates.
In the search for electroweak production of supersymmetry, the di-tau channel is a dominant final state within the light stau models. The taus may decay hadronically or leptonically. An important background to this final state is given by events where other objects are misidentified as leptons ('fake lepton').
This thesis presents measurements of the probabilities for the selected leptons to be either fake or real leptons in various Standard Model processes. The measurement is performed with the 2012 dataset collected with the ATLAS experiment at a center-of-mass energy of $\sqrt{s} = 8$ TeV, corresponding to an integrated luminosity of approximately 20.3 fb^{-1}.

Contents

Chapter 1

Introduction

Since the 1930s many theories and discoveries have resulted in the idea that everything in the universe is made from a few basic particles and interacts via four fundamental forces. In the early 1970s a theoretical model that describes these particles and three of the fundamental forces has been developed. This model is the so-called Standard Model.
The Standard Model of particle physics is one of the most successful theories and is studied in detail till today. However, even though the SM is currently the best description of the subatomic world, it includes several open issues and problems which indicate that there is physics beyond it.
Most of the elementary particles are not stable and therefore no longer present in nature. In order to explore their properties they are produced in an artificial way by colliding two beams of stable particles with high energies via particle accelerators.
The Large Hadron Collider (LHC) is the largest particle accelerator in the world, which collides proton beams into a center-of-mass energy of $\sqrt{s} = 8$ TeV. The LHC detector ATLAS is a large multi-purpose detector. One of the main goals of ATLAS is the search for supersymmetric particles.
Supersymmety is a leading extension of the SM which provides solutions to some problems in the model, such as the hierarchy problem and dark matter. Supersymmetry argues that each SM particle has a superparticle partner with 1/2 spin difference with respect to the SM particle. There are many models of supersymmetry, while the Minimal Supersymmetric Standard Model (MSSM) is the model with minimal particle content.
In this thesis a search for supersymmetry in events with two taus and missing transverse energy from p-p collisions at the LHC at $\sqrt{s} = 8$ TeV is presented. The selection criteria described in this thesis are focused on the detection of events in which a pair of supersymmetric particles was electroweakly produced. An efficient search requires the estimation of the Standard Model background with high accuracy. This thesis presents the investigation of the *fake* background, namely the SM background originating from leptons which are mis-identified by the detector.
This thesis is structured as follows. A brief overview of the theoretical background is presented in Chapter 2, including the SM description and supersymmetry guiding lines. In Chapter 3 the experimental setup of the LHC accelerator and the ATLAS detector is described. Chapter 4 gives detailed information of the analysis, describing the datasets, kinematic variables, the reconstruction of particles and event selection criteria which are used in this thesis. In Chapter 5 an estimation

of the origin of reconstructed leptons within the desirable final state is presented. Chapter 6 describes the estimation of the efficiencies of the fake background in data, based on Monte Carlo simulations for each SM background. The Matrix Method, a method for fake background estimation based on data is introduced in Chapter 7. Within this chapter the method is described and its implementation on data is presented.

Chapter 2

Theoretical Foundations

In this chapter the theoretical fundamentals for this thesis will be described. We begin with a brief description of the Standard Model based on [1] and [2], then present the difficulties arising from the model [3], and follow this with an introduction to the Supersymmetry as a possible extension of the Standard Model based on [4] and [5].

2.1 The Standard Model of Particle Physics

The Standard Model (SM) of particle physics is a successful theoretical framework which describes nature at small scales. It has been developed in the second half of the 20^{th} century.
The Standard Model describes a small group of particles with spin 1/2, which form all known matter. These elementary particles are denoted by the name fermions since they obey Fermi-Dirac statistics. The fermions interact via force carrier particles, the gauge bosons. Gauge bosons are integer spin particles which obey Bose-Einstein statistics.
Fermions are divided into two groups: leptons and quarks.
The leptons are classified via their charge (Q), electron number (L_e), muon number (L_μ), and tau number (L_τ). They fall into three generations:

Generation	Lepton	Mass [MeV]	Q	L_e	L_μ	L_τ
1^{st} generation	e (electron)	0.511	-1	1	0	0
	ν_e (e neutrino)	≤ 0.002	0	1	0	0
2^{nd} generation	μ (muon)	105.66	-1	0	1	0
	ν_μ (μ neutrino)	$\leq$0.19	0	0	1	0
3^{rd} generation	τ (tau)	1776.82$\pm$0.16	-1	0	0	1
	ν_τ (τ neutrino)	$\leq$18.2	0	0	0	1

Table 2.1: Lepton Properties [6].

There are also six anti-leptons with opposite sign additive charges.
The tau and the muon are unstable.

Similarly, there are six quarks which are also separated into three generations. They are characterized by charge (Q), upness (U), downness (D), strangeness (S), charm (C), beauty (B) and truth(T). The quarks and their properties are listed in Table 2.2.

Generation	Quark	Mass [GeV]	Q	D	U	S	C	B	T
1^{st} generation	d (down)	0.0041-0.0058	-1/3	-1	0	0	0	0	0
	u (up)	0.0017-0.0033	2/3	0	1	0	0	0	0
2^{nd} generation	s (strange)	101^{+29}_{-21}	-1/3	0	0	-1	0	0	0
	c (charm)	$1.27^{+0.07}_{-0.09}$	2/3	0	0	0	1	0	0
3^{rd} generation	b (bottom)	$4.19^{+0.18}_{-0.06}$	-1/3	0	0	0	0	-1	0
	t (top)	$172 \pm 0.9 \pm 1.3$	2/3	0	0	0	0	0	1

Table 2.2: Quark Properties [6].

As for the leptons, each quark corresponds to an anti-quark with the same mass, however with reversed sign additive charges.
The interactions between fermions are mediated via forces. As far as we know, there are four fundamental forces in nature: strong, electromagnetic, weak and gravitational. Table 2.3 presents an overview of these forces and their mediating bosons sorted according to the forces relative strength.

Force	Relative Strength	Theory	Gauge Boson
Strong	1	Chromodynamics	8 Gluons, g
Electromagnetic	1/137	Electrodynamics	Photon, γ
Weak	10^{-14}	Flavourdynamics	W^+, W^-, Z^0
Gravitational	10^{-40}	Gravity	Graviton, G

Table 2.3: The Fundamental Forces and their Gauge Bosons.

Each interaction can be described via a physical theory. The theories are, except for the gravitational interaction, Quantum Field Theories (QFT).

- The strong interaction is described by Quantum Chromodynamics (QCD). This interaction is responsible for binding the quarks inside protons and neutrons. It has eight mediators, gluons, which differ by their colours and can interact only with coloured particles (quarks and gluons).

- The electromagnetic (EM) interaction is described by Quantum Electrodynamics (QED). It produces electromagnetic waves and chemical binding in atoms and molecules. The photon is the mediator for EM interaction and it interacts only with charged particles.

- The weak interaction takes part in certain decays, including β decay. It has two charged mediators W^- and W^+. It was extended to the electroweak interaction (unification of electromagnetic interaction and weak interaction) with an additional neutral mediator, the Z boson. The electroweak interaction is described by Quantum Flavourdynamics (QFD).

- Gravitational interaction acts between all types of massive particles. It is classically described by Newton's law of gravity. Although it is the weakest of all the fundamental interactions, it is strongly dominant on the scale of the universe. This interaction is not part of the Standard Model, since fitting it into this framework has proven to be a difficult challenge. The graviton should be the corresponding force carrier of gravity, yet so far it has not been found.

All of the interactions obey several conservations laws. From kinematic conservations of energy, momentum and angular momentum to charge, colour, quark number, flavour (except for weak interaction) and lepton number conservations.

Physical systems can be described by the Lagrangian density $\mathcal{L}$. $\mathcal{L}$ is a function of fields (ψ^i) and their space-time derivatives ($\frac{\partial \psi^i}{\partial x_\mu}$, $\mu = t, x, y, z$). Quantum field theories in the Standard Model are gauge theories. In Gauge theories $\mathcal{L}$ is required to be invariant under local gauge symmetries ($\psi \to e^{i\theta(x_\mu)}\psi$, where θ is a function of x_μ).

The fundamental gauge symmetries for the SM model are: $U(1)_Y \otimes SU(2)_L \otimes SU(3)$. $U(1)_Y \otimes SU(2)_L$ represents the symmetry group of the electroweak theory, a unified theory for the electromagnetic and the weak interactions, developed by Glashow, Weinberg and Salam (GWS theory). The Y symbolizes the hyper-charge Y, a united charge for electromagnetic and weak interactions, and the L symbolizes the parity violation in the weak interaction (only left-handed fermions participate). $SU(3)$ is the symmetry group of QCD.

When implementing gauge symmetry,massive gauge fields impose problems. This difficulty does not arise for the strong and electromagnetic interactions, since photons and gluons are indeed massless. However, a problem arose in weak interactions. The force mediators of the weak interaction were found to be massive in experiments. GWS theory together with the Higgs mechanism provides the solution.
The GWS theory starts with four massless mediating bosons for the electroweak interaction. In a procedure called spontaneous symmetry breaking, a complex scalar

field ϕ in the form

$$\phi = \begin{pmatrix} \phi^+ \\ \phi^0 \end{pmatrix} \qquad \phi^\dagger = \begin{pmatrix} \phi^0 \\ \phi^- \end{pmatrix} \tag{2.1}$$

is introduced, where ϕ^+ and ϕ^- are charged and ϕ^0 and $\phi^{\dagger 0}$ are neutral.
This field is the Higgs field which has non-zero vacuum expectation values. The Higgs coupling to gauge fields yields three massive weak bosons, $W^\pm$ and Z, and one massless photon. Moreover, the interaction between the Higgs field and the fermions generates the fermion masses.

2.2 Open Issues Concerning the Standard Model

So far the Standard Model (SM) has been highly successful and provides a good prediction of the fundamental interactions between particles according to experimental observation. The last experimental contribution to the model was the discovery of a Higgs boson at the ATLAS [7] and CMS [8] experiments in 2012.
However, there are several open issues and problems with the Standard Model.
First, the SM includes 19 free parameters, which can only be determined by experimental measurements. It does not explain the parity violation in the electroweak interaction, nor the charge quantization in nature, i.e. why all particles carry charges which are multiples of $e/3$. The existence of three generations of fermions has no explanation, likewise the hierarchical pattern of their masses. Furthermore, astronomical evidences indicate that only $\sim 5\%$ of the mass/energy content of the universe consists of the matter described by the Standard Model. The rest is dark energy ($\sim 68\%$) and dark matter ($\sim 27\%$).

The successful electroweak theory motivated a development of more general unification theories, which combine the electroweak and strong interactions, the so-called Grand Unified Theories (GUT). According to GUT, the unification of all known interactions is described by one interaction associated with a simple gauge group. The unification occurs at very high energy scale ($\sim 10^{16}$ GeV), and at this scale the coupling strengths of the interactions should reach the same value. This is impossible to achieve within the SM framework, however in other models such as the MSSM, it can be achieved (see Figure 2.2).
Another problem in the Standard Model is the hierarchy problem. Due to theoretical arguments, the mass of the Higgs boson should not be too different from the W boson mass. On the other hand, when calculating the mass at higher orders, radiative corrections are taken into account and Higgs mass becomes dependent on the next higher scale in the theory Λ. Then the Higgs mass is defined in the form

$$M_H^2 = (M_H^2)_{1^{st}order} + \mathcal{O}(\lambda, g^2, h^2)\Lambda^2 \tag{2.2}$$

where λ, g and h denote the coupling parameters for Higgs fields as Figure 2.1 describes. Λ would be the Planck scale, $M_P \sim 10^{19}$ GeV, if gravity is the next scale, or the $\sim 10^{16}$ scale, if GUT exists. In any case, the large difference between the scales would create an unstable mass value, unless a precise cancellation between the two scales exists.

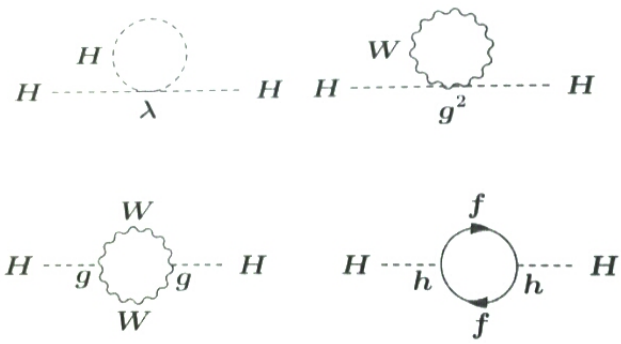

Figure 2.1: Radiative corrections to the Higgs mass, including self-interactions,interactions with gauge bosons, and interactions with fermions. [3]

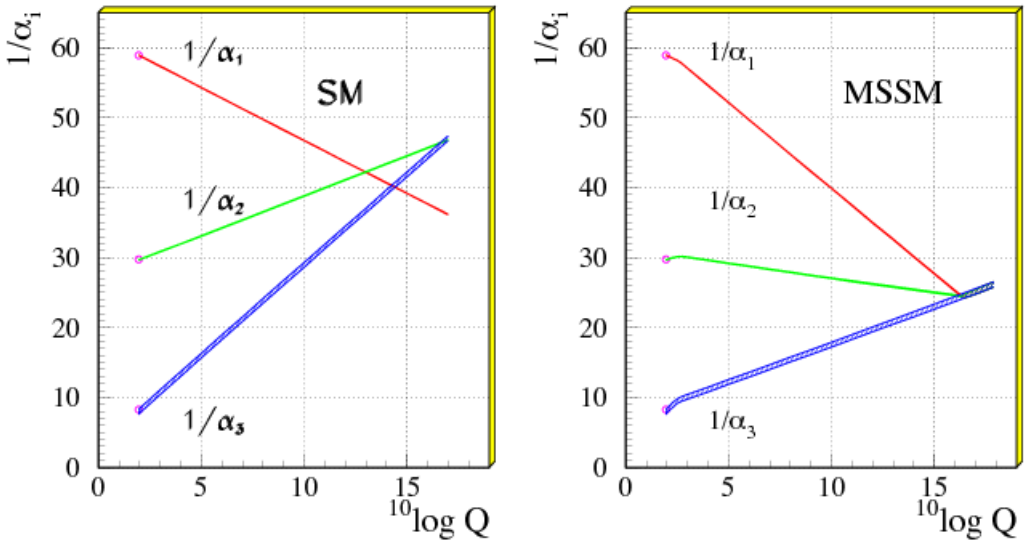

Figure 2.2: Evolution of the inverse of the three coupling parameters in the Standard Model (left) and in the MSSM (right). α_1, α_2 and α_3 correspond to the U(1), SU(2) and SU(3) gauge coupling parameters [9].

2.3 Supersymmetry

Supersymmetry (SUSY) is one of the most promising extensions of the Standard Model. The supersymmetry theory provides possible solutions to the Standard Model problems and is one of the candidates for a unified theory beyond it. The SUSY framework brings a solution to the hierarchy problem and offers a dark matter candidate.
The theory describes a space-time symmetry between bosons and fermions using an operator Q that turns a bosonic state into a fermionic state, and vice versa.

$$Q\,|Boson\rangle = |Fermion\rangle \qquad\qquad Q\,|Fermion\rangle = |Boson\rangle \tag{2.3}$$

The operator Q must be an anticommutaing spinor and so its hermitian conjugate $Q^\dagger$ is also a supersymmetry generator. These operators are called fermionic operators

because of the spin 1/2 which they carry. Supersymmetry algebra goes together with parity-violating interactions and as such must have the following commutation and anticommutation relations

$$\{Q_s, Q_r^\dagger\} = -2\sigma_{sr}^\mu P_\mu \tag{2.4}$$
$$\{Q_s, Q_r\} = 0 \tag{2.5}$$
$$\{Q_s^\dagger, Q_r^\dagger\} = 0 \tag{2.6}$$

where P^μ is the four momentum generator of space-time translations and σ_{sr}^μ are the Pauli matrices.
In supersymmetry algebra, a supermultiplet is a set of states with the same representation of a gauge group: electric charges, weak isospin and color degree of freedom. Each supermultiplet contains the fermionic and bosonic states, which are known as superpartners of each other. By definition each superpartner is proportional to some combination of the Q and $Q^\dagger$ operators, acting on its partner. The supersymmetry operators commute with the squared-mass operator $-P^2$, as the other space-time operators. Consequently, the superpartners must have equal eigenvalues of $-P^2$, namely the same masses.

In supersymmetry, the fermions have spin-0 superpartners, which are called sfermions (the 's' stands for scalar). Each superpartner is marked with the same symbols as the corresponding particle, but with a tilde on top. For example, the superpartner of a right-handed electron e_R is denoted as $\tilde{e}_R$.
The SM gauge bosons carry spin 1. They have spin 1/2 superpartners which are called gauginos. It is important to note that neither fermionic nor bosonic states would gain mass before the gauge electroweak symmetry is spontaneously broken.
Supersymmetry theory includes two supermultiplets for two Higgs fields, H_u and H_d, and their fermionic superpartners, the higgsinos $\tilde{H}_u$ and $\tilde{H}_d$. H_u is responsible for generating masses of the up-type quarks (u, c, t) and H_d generates masses of down-type quarks (d, s, b).
In supersymmetric models which include gravity, the superpartner of the spin-2 graviton is the spin-3/2 gravitino.

The SM hierarchy problem, which has been mentioned before, can be solve in the supersymmetry framework. For example, a correction to M_H^2 from an interaction with fermion f with mass m_f, coupled with coupling parameter λ_f, would yield a correction of the form

$$\Delta m_H^2 = -\frac{|\lambda_f^2|}{8\pi^2}\Lambda^2 + ... \tag{2.7}$$

Supersymmetry introduces two complex scalar fields S with mass m_S for each Standard Model fermion. They are coupled to the Higgs with λ_S and each yields a correction of

$$\Delta m_H^2 = \frac{\lambda_S}{16\pi^2}\left[\Lambda^2 - 2m_S^2 \ln\left(\frac{\Lambda}{m_S}\right) + \mathcal{O}\left(\frac{1}{\Lambda^2}\right)\right]. \tag{2.8}$$

When we combine these corrections, we get

$$\Delta m_H^2 = \frac{1}{8\pi^2}\left(\lambda_s - |\lambda_f|^2\right)\Lambda^2 + ... \tag{2.9}$$

Then, by requiring a relation between the coupling parameters (for example $\lambda_S = |\lambda_f|^2$), the quadratical dependence on Λ gets cancelled.

From the description of SUSY so far, it seems that superpartners have the same mass as their partners. If this was the case, then selectrons with masses of $m_e = 0.511$ MeV would already be detected. Nevertheless, none of the superpartners of the Standard Model particles has been discovered as of this writing. Therefore supersymmetry must be broken in order to allow the superpartners to acquire large masses.

2.4 MSSM

The Minimal Supersymmetric Standard Model (MSSM) is a supersymmetric version of the Standard Model with minimal particle content. The particles are summarized in Table 2.4.

Bosons		Fermions	
gluon	g	gluino	$\tilde{g}$
weak	$W^{\pm}$, Z	wino, zino	$\tilde{w}^{\pm}$, $\tilde{z}$
hyper-charge	B^0	bino	$\tilde{B}^0$
sleptons	$\tilde{\nu}_L$, $\tilde{e}_L$	leptons	ν_L, e_L
	$\tilde{e}_R$		e_R
squarks	$\tilde{u}_L$, $\tilde{d}_L$	quarks	u_L, d_L
	$\tilde{u}_R$		u_R
	$\tilde{d}_R$		d_R
Higgs	H_1	higgsinos	H_1
	H_2		H_2

Table 2.4: Particle Content of the MSSM

The MSSM uses a special symmetry called the R-parity [10] which is defined by

$$R = (-1)^{3(B-L)+2S} \tag{2.10}$$

where B is the baryon number, L is the lepton number, and S is the spin of the particle. Conservation of R-parity leads to pair production of superparticles and to a stable lightest supersymmetric particle (LSP), which makes the LSP an excellent candidate for the Dark Matter particle.

Due to the effects of electroweak symmetry breaking, the higgsinos and the electroweak gauginos mix with each other. The neutral higgsinos ($\tilde{H}_u^0$ and $\tilde{H}_d^0$) and the neutral gauginos ($\tilde{B}^0$ and $\tilde{z}$) form four mass eigenstates called neutralinos. The charged higgsinos ($\tilde{H}_u^+$ and $\tilde{H}_d^-$) and the winos ($\tilde{w}^\pm$) mix to form four mass eigenstates with charge ± 1 called charginos. The neutralinos are referred to as $\tilde{\chi}_i^0$ (i=1,2,3,4) and charginos are denoted as $\tilde{\chi}_i^\pm$ (i=1,2). The lightest neutralino, $\tilde{\chi}_1^0$, is assumed to be the LSP.
In the MSSM there are no fields with non-zero vacuum expectation values which are required for spontaneous SUSY breaking. This points to the existence of another field which is responsible for the spontaneous supersymmetric breaking. In that case the effective Lagrangian of the MSSM can be written in the form

$$\mathcal{L} = \mathcal{L}_{SUSY} + \mathcal{L}_{soft} \tag{2.11}$$

where $\mathcal{L}_{SUSY}$ stands for the unbroken SUSY theory and $\mathcal{L}_{soft}$ represents the term with the SUSY breaking field.
Together with the symmetry breaking arises the question if broken SUSY still provides a solution for the hierarchy problem. The Lagrangian in equation 2.11 yields an additional correction to M_H^2 from the soft field. It is possible to derive the additional correction via dimensional analysis, when considering m_{soft} as the largest mass scale associated with the soft terms. The correction would be

$$\Delta m_H^2 = m_{soft}^2 \left[\frac{\lambda}{16\pi^2} \ln\left(\frac{\Lambda}{m_{soft}}\right) + ... \right] \tag{2.12}$$

where λ denotes various coupling parameters. From equation 2.12 it is clear that the correction to the Higgs mass remains small if the superpartner masses are not too large. If we use $\Lambda \sim M_P$ and $\lambda \sim 1$, we can estimate that the lightest superpartners should have masses at scales close to the TeV scale. This energy range is accessible at the LHC.

Chapter 3

Experimental Setup

3.1 The Large Hadron Collider

The Large Hadron Collider (LHC) is a synchrotron-type accelerator and collider operated by the European Organization for Nuclear Research (CERN) in Geneva, Switzerland. It is the largest and most powerful collider in the world, with a circumference of 26.7 km, located at the border between Switzerland and France.
The LHC is designed to collide proton (p) beams or lead (Pb) beams at unprecedented energies and luminosities. It aims at finding solutions to the problems of the Standard Model and exploring physics beyond it. Special efforts are dedicated to probe the existence of the Standard Model Higgs boson. In 2012, a great progress was achieved with the discovery of a Higgs boson by ATLAS [7] and CMS [8].

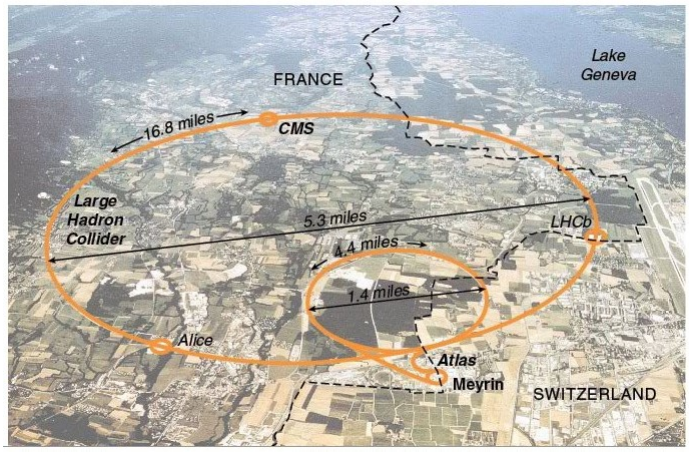

Figure 3.1: LHC on the map [11].

LHC is designed for proton collisions at a center-of-mass energy of $\sqrt{s} = 14$ TeV at a luminosity of $L = 10^{34}\ cm^{-2}s^{-1}$ [12]. The first p-p collisions in November 2009 reached to a center-of-mass energy of 900 GeV. Since then the beam energy has been increased to form a higher center-of-mass energy, achieving $\sqrt{s} = 7$ TeV in 2010, and $\sqrt{s} = 8$ TeV in 2012. From the end of 2012 until 2014, LHC undergoes a maintenance phase to reach its full design center-of-mass energy - 14 TeV.

Four major experiments are located along the LHC ring. The biggest of these experiments, ATLAS (A Toroidal LHC Apparatus) and CMS (Compact Muon Solenoid), are multi purpose detectors, investigating a wide range of physics, while ALICE (A Large Ion Collider Experiment) and LHCb (Large Hadron Collider beauty) are specialized detectors for specific phenomena. In addition, smaller experiments are located within the experimental halls of the large detectors.

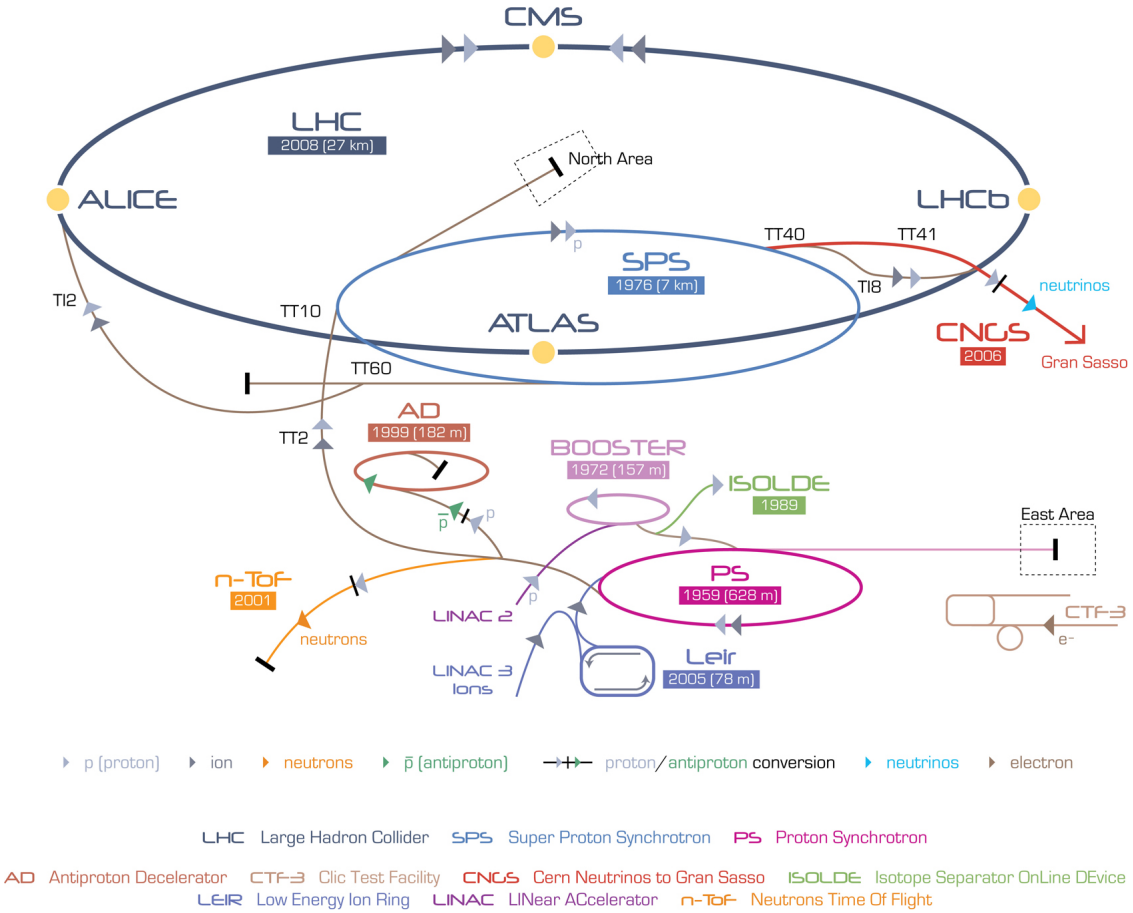

Figure 3.2: CERN accelerator complex [13].

3.2 The ATLAS Detector

The ATLAS detector has been built for probing *p*-*p* and heavy ion collisions performed by the LHC. It is intended to produce high precision measurements, contributing to many fields of research such as the Higgs boson and its properties and the search for supersymmetric particles. The main challenges in the detector design were detecting a broad range of physics signals and the high disturbing radiation from LHC. Therefore, the design required radiation hard components with maximum sensitivity and fast response time.

ATLAS is arranged in a layered structure around the collision point, combining different sub-detectors, as can be seen in Figure 3.3. The first layer around the beam pipe is the Inner Detector. It is used to reconstruct the trajectory of charged

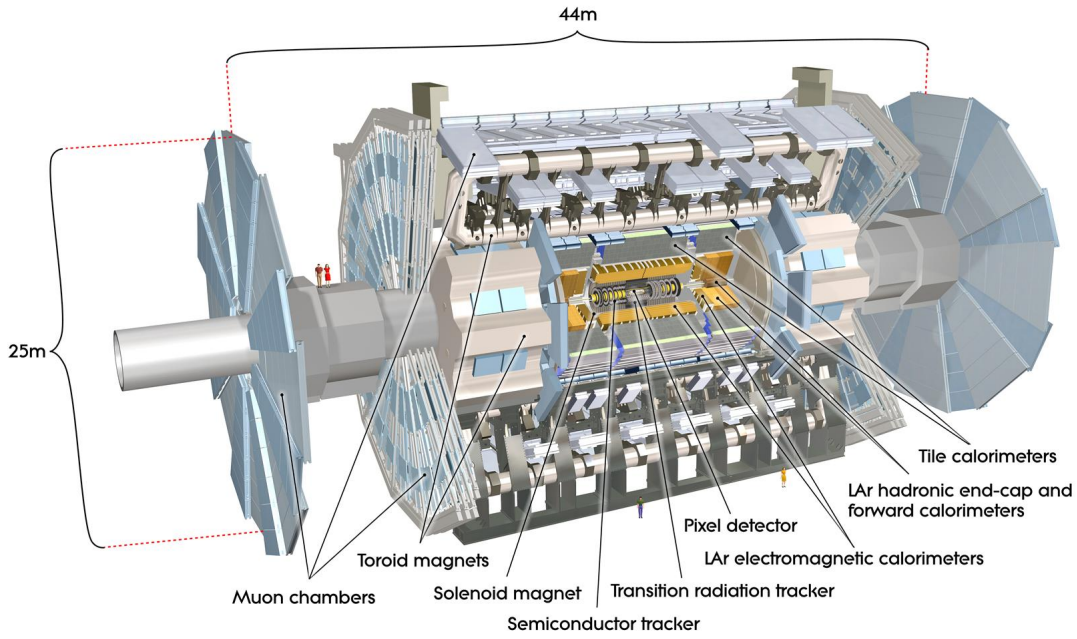

Figure 3.3: The ATLAS detector composition [15].

particles and to measure the particle momentum and charge. The Inner Detector is surrounded by a superconducting solenoidal magnet to measure the momenta of charged particles. The next sub-detectors are two calorimeters, Electromagnetic and Hadronic Calorimeters, which measure the energies carried by the particles. Finally, the Muon Spectrometer which is designed to reconstruct and identify muons.
A brief description of the ATLAS system is given in the following sections, more detailed accounts can be found in [14].

3.2.1 Coordinate System

The ATLAS coordinate system defines a forward-backward symmetry in the detector. The origin of the coordinate system is set to the nominal interaction point. The axes form a right handed cartesian coordinate system, where the z axis is parallel to the beam, the x axis points towards LHC center, and the y axis points upwards. The azimuthal angle ϕ is measured around the beam axis, and the polar angle θ is measured from the beam axis.
The transverse plane is defined to be the x-y plane, where some kinematic quantities like the transverse momentum $\vec{p}_T$ and transverse energy $\vec{E}_T$ are measured. An additional property measured in the transverse plane is the transverse missing energy $\vec{E}_T^{miss}$. It is defined to be the vectorial sum of the transverse energy of all the particles in the event multiplied by (-1), $\vec{E}_T^{miss} = -\sum_{i \in particles} \vec{E}_{Ti}$[1].
The pseudorapidity, defined as $\eta = -ln\tan(\theta/2)$, is commonly used as a polar coordinate. The distance in the η-ϕ space is defined as $\Delta R = \sqrt{\Delta\eta^2 + \Delta\phi^2}$.

[1]For convenience the vector notation $\vec{}$ is discarded from now on.

3.2.2 The Inner Detector

The Inner detector is built from three independent sub-detectors, all contained in the Central Solenoid (CS). The CS provides a nearly uniform magnetic field of 2T which bends the trajectory of charged particles in the transverse plane. The track curvature is used to measure the particle p_T, while the sign of the curvature is used for charge measurements.
The Pixel Detector is the closest component to the beam line, located in the region with the highest particle density. In order to provide precise measurements of the primary and secondary vertex as well as particles tracks, it is required to have a very high spatial resolution. The Semiconductor Tracker (SCT) is the next layer within a region of reduced particle density, and therefore satisfies less strict demands on occupancy. Both detectors are made from semiconductor technology, which is radiation hard. The third detector is the Transition Radiation Tracker (TRT), which consists of long straw-tubes filled with gas. Each tube has a wire in the middle, which is collecting the ions produced by the charged particle. This process allows a space-point measurement of the particle track.
The tracks are described by five parameters which are estimated from the reconstruction: $1/p_T$, ϕ, θ, d_0 and z_0. d_0 measures the closest approach to the interaction point in the transverse plane, while z_0 measures the closest approach to the beam axis. The track reconstruction combines measurements from all three sub-detectors with a high-precision parameter estimation.

3.2.3 Calorimeters

The calorimeter systems covers a measurement range of $|\eta| < 4.9$. Calorimeters are designed to provide good containment for the electromagnetic and hadronic showers for precise measurement of the deposited energy and to reduce punch-through into the Muon Spectrometer. For this reason the total thickness of the system is an important parameter, which also ensures a good E_T^{miss} measurement.
The Electromagnetic Calorimeter has a fine granularity which enables precise measurements of electrons and photons. It is a lead-LAr[2] detector with accordion shape absorbers and electrodes. The accordion geometry guarantees high resolution in ϕ.
The Hadronic Calorimeter is designed to satisfy the physics requirements for jet reconstruction and E_T^{miss} measurements. It contains three sub-calorimeters for maximum η coverage: the Tile Calorimeter, the LAr Hadronic End-cap Calorimeter (HEC) and the LAR Forward Calorimeter (FCal). The sub-calorimeters setup can be seen in Figure 3.4. The Tile Calorimeter uses scintillating tiles as active material and steal as absorber; the HEC and Fcal use LAr as active material and copper as absorber, while HEC uses in some parts tungsten instead of copper.

[2]LAr - liquid-argon.

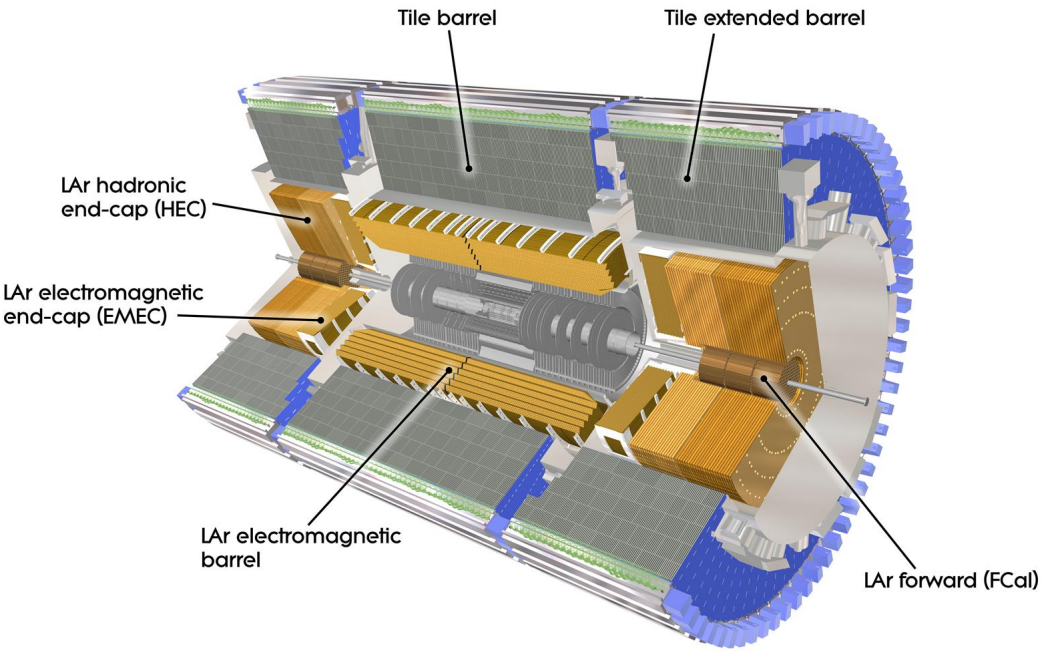

Figure 3.4: Cut-away view of the ATLAS calorimeter system [15].

3.2.4 The Muon Spectrometer

Within the calorimeter system, all interacting particles shower, except for the muons. The muons are minimum ionizing particles and therefore loose very little energy when passing through the calorimeters. Direct measurement of their energy is unachievable, hence a 4-momentum is determined from tracking.
The muon system uses large superconducting air-core toroid magnets in order to bend the muon paths. The paths are measured by a system of drift tubes.
The Muon Spectrometer covers a region of $|\eta| < 2.7$. It consists of four subsystems. The Monitored Drift Tube Chambers (MDT's) and Cathode-Strip Chambers (CSC's) provide precise measurements of the tracks. In addition, the Resistive Plate Chambers (RPC's) and the Thin Gap Chambers (TGC's) are fast trigger chambers with rapid response time of a few tens of nanoseconds.

Figure 3.5 illustrates the detection of particles in the ATLAS sub-detectors system.

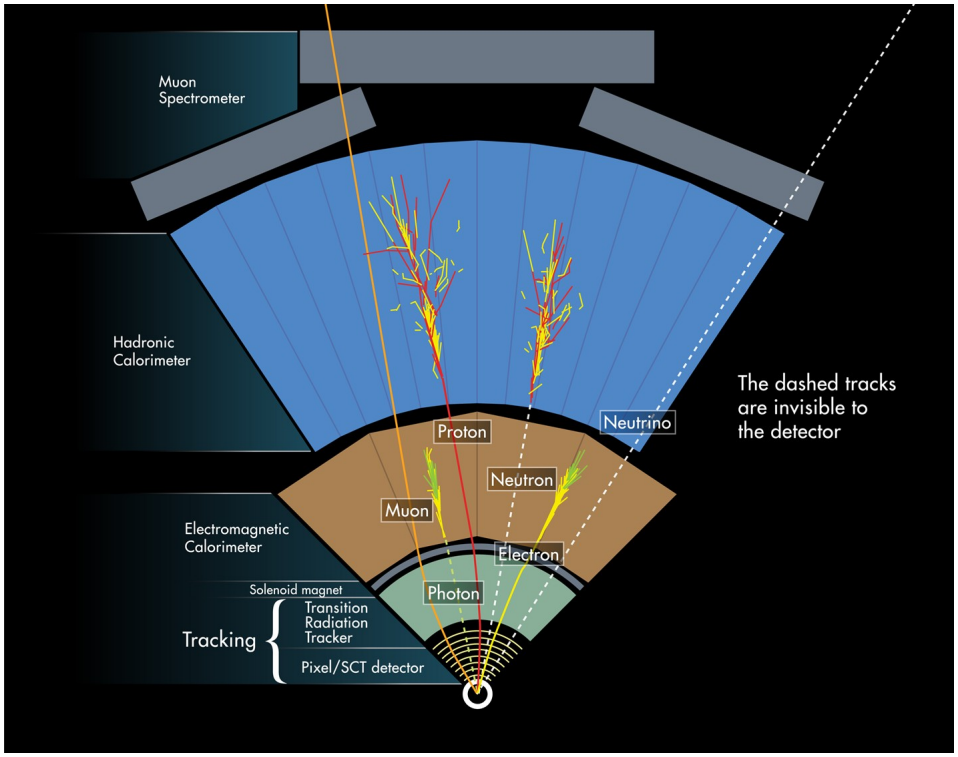

Figure 3.5: Particle detections in the ATLAS layers structure [15].

3.3 Trigger and Data Acquisition

The p-p interaction rate, at the full design luminosity of LHC, is approximately 1 GHz, however the total recording rate of ATLAS is limited to a few hundred Hz. In order to reduce the high rate to an acceptable level, a three level trigger system is installed. The system is designed to maximize the selection efficiency of interesting physics signals.
The Level 1 Trigger (L1) is a hardware based trigger, which integrates information from the calorimeters and the Muon Spectrometer. It selects events with large E_T^{miss} and high p_T objects, and defines the Regions-of-Interest (ROI's) of the detector. The L1 Trigger reduces the event rate to about 75 kHz. The Level 2 Trigger (L2) is a software based trigger which performs a further selection within ROI's according to the available data from all sub-detectors. It has a nominal average processing time of 40 ms and it reduces the output rate to around 3 kHz. The last element in the trigger system is the Event Filter, which uses software processors to achieve reduction of the rate to the final write-out frequency of a few hundred Hz.

3.4 The Worldwide LHC Computing Grid

The huge volume of recorded data and the need to share access amongst the many institutes in different countries motivated the establishment of the Worldwide LHC Computing Grid (WLCG) [16, 17]. WLCG is a global collaboration of computer centers, organized in four levels called Tiers.
Tier-0 is located at CERN and receives all the data from LHC detectors, namely the raw events. It performs the first processing into meaningful information and distributes the raw data and the reconstructed output to the Tier-1 centers.
The Tier-1 centers include twelve computing centers worldwide. These computing centers can store the raw data as well as perform a further processing to derive datasets. The Tier-1's also provide a facility for scheduled access to large quantities of data. They take part in the experiment reprocessing and host file catalogues and file transfer services. Tier 1s are linked to each other and to CERN by a dedicated Optical Private Network.
The Tier-2 facilities are spread between universities and other scientific institutes which take part in the experiments. During early data taking, Tier 2 sites reconstruct small samples of events with developing calibrations or algorithms. In addition, they store datasets and provide the main simulation capacity for the experiment.
The Tier-3's are computing resources accessible to individual scientists, which can consist of local clusters in a university department or even individual PCs. They are intended to make capacity available for simulation on a temporary basis.

Chapter 4

Analysis

This thesis aims to study the fake background in the di-tau channel in the search for electroweakly produced supersymmetry. Fake background arises from mis-reconstructed objects that pass the object selection. This chapter presents the basic outlines of the analysis: the relevant SUSY models, the studied final state, the datasets that were used and the event and object selection.

4.1 Studied SUSY Scenario

In R-parity conserving SUSY models, SUSY particles are produced in pairs and the Lightest Supersymmetric Particle (LSP) is stable and weakly interacting.
In several models the charginos and neutralinos, as well as sleptons can be sufficiently light to be produced at the LHC. If the coloured sparticles (squarks and gluinos) are sufficiently heavy, the first SUSY sign may be detected in the direct production of charginos, neutralinos and sleptons, namely in the supersymmetric electroweak production.

This analysis uses models where the lightest neutralino $\tilde{\chi}_1^0$ is assumed to be the LSP, while the charginos and the other neutralinos, $\tilde{\chi}_i^{\pm}$ (i=1,2) and $\tilde{\chi}_j^0$ (j=2,3,4), are assumed to be heavier than the tau slepton $\tilde{\tau}$. In general, light slepton could play a role in the co-annihilation of neutralinos, leading to dark matter relic density consistent with cosmological observations [18, 19]. In this analysis, models where the stau is the only light slepton are used.

The Phenomenological Minimal Supersymmetric Standard Model (pMSSM) is a framework which supports such a scenario. In the pMSSM, the dominant electroweak production channels with at least two leptons in the final state are chargino-chargino production ($\widetilde{\chi}_1^{\pm}\widetilde{\chi}_1^{\mp}$) and chargino-neutralino production ($\widetilde{\chi}_1^{\pm}\widetilde{\chi}_2^0$).
For the case that the $\widetilde{\chi}_1^{\pm}$ and $\widetilde{\chi}_2^0$ are heavier than the stau and the tau sneutrino, the following decay processes can occur: $\widetilde{\chi}_2^0 \to \widetilde{\tau}\tau \to \tau\tau\widetilde{\chi}_1^0$, and $\widetilde{\chi}_1^{\pm} \to \widetilde{\tau}\nu(\widetilde{\nu}\tau) \to \tau\nu\widetilde{\chi}_1^0$.
The appropriate diagrams for chargino-chargino and chargino-neutralino productions are presented in Figure 4.1.
If charginos and neutralinos are too heavy to be produced at the LHC, the direct production of staus ($\widetilde{\tau}^{\pm}\widetilde{\tau}^{\mp}$) becomes the dominant electroweak production in the pMSSM. The production of stau pairs with decays leading to two taus in the final state is presented in Figure 4.2.

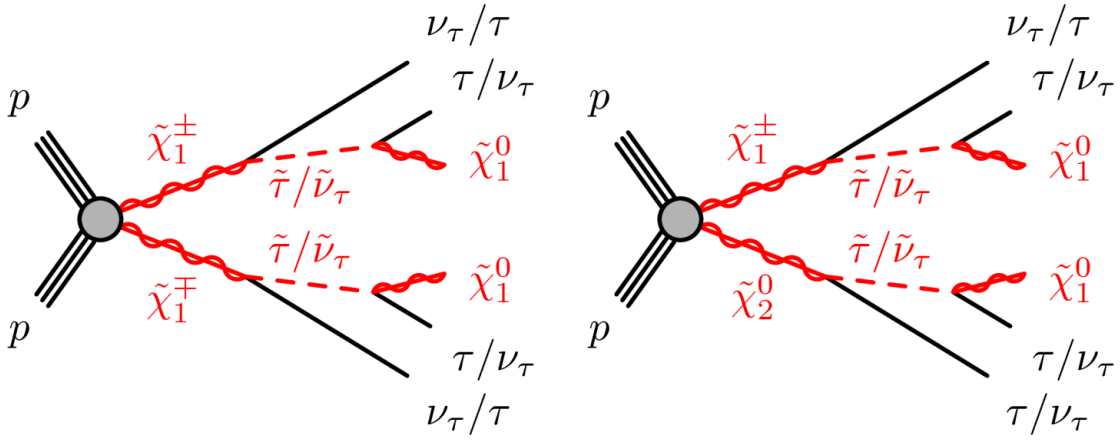

Figure 4.1: Diagrams for $\widetilde{\chi}_1^{\pm}\widetilde{\chi}_1^{\mp}$ (left) and $\widetilde{\chi}_1^{\pm}\widetilde{\chi}_2^0$ (right) decays with intermediate light left-handed charged sleptons and sneutrinos.

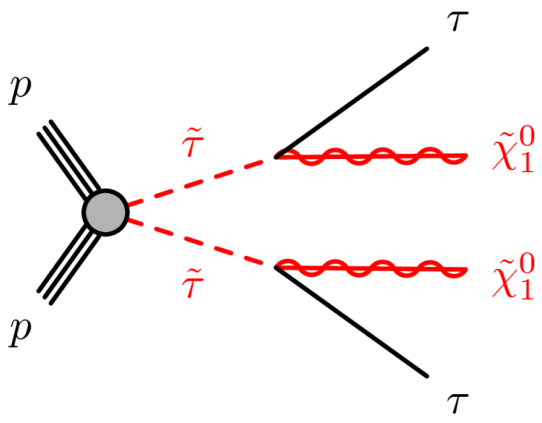

Figure 4.2: Diagram for $\widetilde{\tau}^{\pm}\widetilde{\tau}^{\mp}$ decay.

4.2 The Di-tau Channel

In this thesis, only final states containing exactly two taus are considered. The $\widetilde{\chi}_1^{\pm}\widetilde{\chi}_1^{\mp}$ production, which yields events with two opposite sign (OS) taus, gives the main contribution to the di-tau channel, while $\widetilde{\chi}_1^{\pm}\widetilde{\chi}_2^0$ production yields three taus, but can be taken into account in the case where one tau is not reconstructed or out of the detector acceptance. Another contribution to the final state comes from direct production of staus ($\widetilde{\tau}^{\pm}\widetilde{\tau}^{\mp}$), which also yields two OS taus in the final state. This analysis restricts the selection of the taus according to their decays and focuses only on events where one of the taus decays hadronically, whereas the other one decays leptonically.
Taus are unstable particles with a short lifetime and will decay long before reaching any of the ATLAS detectors. Therefore for tau reconstruction it is necessary to

use their decay products. In ATLAS it is not possible to distinguish a leptonic tau decay from a prompt lepton because there is no dedicated algorithm for leptonically decaying taus. On the other hand, hadronically decaying taus can be reconstructed as well as light leptons. In this analysis, it is assumed that leptonically decaying taus are reconstructed in the form of light leptons. Consequently, the analysis is based on recorded events with one tau, one light lepton (muon or electron) and missing transverse energy.

4.3 SM Background

The main background to the di-tau channel arises from five different SM processes: W+jets, Z+jets, diboson, $t\bar{t}$ and multi-jet production.

- W+jets processes - the decay of the W boson can produce one lepton with the corresponding neutrino and a mis-identified jet can be detected as a second lepton.
- Z+jets processes - the Z boson can decay into two OS leptons with the same flavour.
- Diboson processes - in all variations of diboson leptonic decays, two to four leptons may be produced.
- $t\bar{t}$ processes - top quarks decay into a W boson and a bottom quark. Since the W boson can decay either hadronically or leptonically, in $t\bar{t}$ production there are several possible decays. In fully leptonic $t\bar{t}$ decays, two leptons would be produced. However in semileptonic decays, one lepton comes from the W decay, while the second lepton originated from b-jet decay or from mis-identified jets.
- Multi-jet processes - dilepton events can be found in multi-jet events when two jets are mis-identified as leptons.

4.4 Datasets

4.4.1 Data

This thesis is based on measurements from the ATLAS experiment in p-p collisions at a center-of-mass energy of $\sqrt{s} = 8$ TeV in 2012, corresponding to an integrated luminosity of approximately 20.3 fb^{-1}. The data quality is being monitored, thus only events which pass a certain quality level are taken into account.

4.4.2 Monte Carlo

Monte Carlo (MC) generators are used to simulate events from LHC collisions. They are processed through a detailed detector simulation [20] based on `GEANT4` [21] and reconstructed using the same algorithms as the data, with the effect of multiple proton-proton collisions in the same or nearby bunch crossing (pile-up) also taken

into account.
MC processes are weighted according to their cross sections and normalized to data luminosity.
In this thesis, MC samples are being used to estimate the SM background contributions. A list of the relevant MC generators is presented in Table 4.1. It is very difficult to model multi-jet processes with MC. These processes have a large cross section but a rather small probability for two reconstructed leptons in an event, therefore the multi-jet background is estimated from data.

SM Background Processes	**MC Generators**
W+jets	`ALPGEN` v2.14 [22] , `PYTHIA` v8.165 [23]
Z+jets	`ALPGEN` v2.14 , `PYTHIA`
Diboson	`SHERPA` v1.4.1 [24]
Diboson + gluon-gluon contributions	`gg2WW` v3.1.2 [25]
$t\bar{t}$	`SHERPA` v1.4.1
$t\bar{t} + V(V = W, Z)$	`MadGraph` 5 v1.3.33 [26], `PYTHIA`
Single-top	`MC@NLO` v4.06 (Wt and s-channel) [27, 28, 29] and `AcerMC` v3.8 (t-channel) [30]

Table 4.1: Monte Carlo Generators used in this Analysis.

4.5 Event Selection

As mentioned in Section 4.2, this analysis refers to events with two OS leptons, one hadronically decaying tau and one leptonically decaying tau which is detected as a light lepton. Events with additional leptons are rejected. Furthermore, events are required to pass certain "quality" selections as detailed in Section 4.5.7.
The object selection distinguishes between "baseline" and "signal" objects. The baseline objects are subject to an overlap removal scheme explained in Section 4.5.6. Objects which pass the overlap removal and satisfy additional requirements are defined as signal objects. Specified object selection for this analysis is listed in the following sections. The selection of jets, muons and electrons is based on object selection in the analysis with two hadronically decaying taus in the final state [31].

4.5.1 Jets

Jets are reconstructed from topological clusters as defined in [32]. The anti-k_t algorithm [33] is used with a distance parameter, $R = \sqrt{\Delta\eta^2 + \Delta\phi^2}$ which is measured from the jet candidate axis, set to R = 0.4. The jet energies are calibrated using the Local Hadron Calibration [34]. First, clusters are classified as electromagnetic or hadronic clusters and corrected for the non-compensating nature of the calorimeter. Then starts the jet reconstruction and final jet-level energy calibrations are applied. Baseline jets are selected from jets with $p_T > 20$ GeV and required to pass a loose quality selection in order to reject jets without association to the real energy deposits in the calorimeter, such as non-collision background events, cosmic-ray showers and calorimeter noise. The signal jets are baseline jets after the overlap removal which obey other requirements as detailed below. They are classified in three exclusive

categories: central b-jets, central light jets and forward jets. The first and the second cover the $|\eta| < 2.4$ region, while the last covers the $2.4 < |\eta| < 4.5$ region.

- B-jets (or `B20`) are jets originating from bottom quarks. A b-tagging algorithm [35] is used to identify jets containing a b-hadron decay. The mean nominal b-tagging efficiency is 80%, with a mis-identification rate for light gluon/quark jets of less than 1%. b-jets are required to have $p_T > 20$ GeV.

- Central light jets (or `L30`) are required to have $p_T > 30$ GeV and not be b-tagged jets. They are characterized by an additional property, the jet vertex fraction, JVF, which is determined from the number of associated charged tracks which point to the event primary vertex. For light central jets $|JVF| > 0$ is required if $p_T < 50$ GeV [36] in order to remove jets that originate from pile-up collisions.

- Forward jets (or `F30`) must have $p_T > 30$.

4.5.2 Taus

The reconstruction of hadronically decaying taus is based on information from topological clusters in the electromagnetic and hadronic Calorimeters [37]. The reconstruction algorithm uses jets which are reconstructed by the anti-k_T algorithm with a distance parameter R = 0.4, and have $p_T > 20$ GeV and $|\eta| < 2.47$. Taus are associated to a primary vertex via a dedicated algorithm, known as Tau Jet Vertex Association (TJVA) [38]. The tau cluster is bounded by a cone of $\Delta R \leq 0.2$ around the axis of the tau candidate in the tau vertex coordinate system. For energy calibration, a Monte Carlo based procedure [39] is being used, which scales the hadronic taus energy independently of the jet energy scale.
Baseline taus are required to have $p_T > 20$ GeV, $|\eta| < 2.47$ and a leading track with $|\eta_{leadTrack}| < 2.47$. The most common hadronic decays for tau leptons are decays to either one or three charged pions, a neutrino and often additional neutral pions. Therefore baseline taus are required to have 1 or 3 tracks (prongs) with a total electric charge of $|q| = 1e$. The distinction between hadronically decaying taus and jets or electrons is refined using multivariate identification algorithms [40].
In this analysis, the tau identification is based on the Boosted Decision Tree (BDT) method [41]. The BDT algorithms use as input various track and cluster variables for particle discrimination. A "jet BDT" is used to discriminate taus from jets, and an "electron BDT" to distinguish between electrons and taus. The electron BDT discrimination is applied only to 1-prong taus. From the BDT algorithms, three tau identification criteria can be defined: "loose", "medium" and "tight". For 1-prong taus "loose", "medium" and "tight" have an efficiency of 70%, 60% and 40%, and for 3-prong taus "loose", "medium" and "tight" have an efficiency of 65%, 55% and 35%, respectively. The background rejection factors range from 10 to 40 for the loosest case (70%) and go up to 500 for the tightest (35%). In this analysis, the baseline taus are required to pass the "loose" selection criteria for the jet discrimination and the "loose" selection criteria for the electron discrimination.

Signal taus are required to pass more stringent requirements: they must pass the "tight" selection criteria for the jet discrimination and a muon veto is applied to remove fake tau candidates from muons coinciding with anomalous energy deposits in the calorimeter.

4.5.3 Electrons

Electrons are detected from clusters in the Electromagnetic Calorimeter and from tracks in the Inner Detector, where the tracks and clusters are matched. Thus two measurement are being used. Depending on the number of hits on the electron track, either the η and ϕ values from track or from the electromagnetic calorimeter are used for the position variables of the electron. Baseline electrons are required to pass the "medium++" identification criteria [42] and to have $p_T > 10$ GeV and $|\eta| < 2.47$.
Signal electrons must pass the following requirements:

- Overlap removal with other electrons, jets, muons and taus as described in detail in section 4.5.6.
- Pass `tight++` criteria as described in [42].
- The transverse distance to the event primary vertex, d_0, must satisfy $|d_0/\sigma_{d_0}| < 5$.
- The distance parameter along the beam direction, z_0, must satisfy $|z_0 \times \sin(\theta)| < 0.4$ mm.
- A candidate must pass the following track and calorimeter isolation requirements:
  - When investigating a cone of size $\Delta R = \sqrt{(\Delta\phi)^2 + (\Delta\eta)^2} = 0.3$ around an electron candidate, if the sum of transverse momenta of tracks which are associated to the primary vertex, is larger than 400 MeV, it is required that this sum of transverse momenta should be less than 16% of the electron p_T[1].
  - In a cone of size $\Delta R = 0.3$ around an electron candidate, the sum of the transverse energies of topological clusters, after p_T and energy density corrections are applied, is required to be less than 18% of the electron[2].

4.5.4 Muons

Muons are formed via the STACO algorithm from the combination between reconstructed tracks in the Muon Spectrometer and the corresponding tracks in the Inner Detector. The analysis includes two types of muons: "combined" muons are reconstructed from tracks in the muon system that match tracks the Inner Detector, while "segment-tagged" muons are reconstructed only from tracks in the Inner Detector

[1]Marked as $p_T cone30/p_T < 0.16$ in Table 4.2. $p_T cone30$ denotes the sum of the p_T within a cone of size $\Delta R = 0.3$.

[2]Marked as $E_T cone30^{\text{corr}}/p_T < 0.18$ in Table 4.2. $E_T cone30$ denotes the sum of the E_T within a cone of size $\Delta R = 0.3$.

and tagged via the muon system.
Baseline muons are required to have $p_T > 10$ GeV, $|\eta| < 2.4$ and to pass the standard muon requirements on the the number of hits in Pixel, SCT and TRT detectors. In addition, the measured transverse momentum in the Inner Detector must be in agreement with the Muon Spectrometer measurements. Muons from cosmic radiation, called "Cosmic Muons", are rejected via tight requirements on the longitudinal impact parameter, $|z_0| < 1.0$ mm, and the transverse impact parameter, $|d_0| < 0.2$ mm, which are both measured with respect to the reconstructed primary vertex. Furthermore, events with badly measured muons (called "Bad Muon") are rejected. Signal muons also need to fulfill the following requirements:

- Overlap removal with other electrons, jets, muons and taus as described in detail in section 4.5.6.
- The transverse distance to the event primary vertex, d_0, must satisfy $|d_0/\sigma_{d_0}| < 3$.
- The distance parameter along the beam direction, z_0, must satisfy $|z_0 \times \sin(\theta)| < 1$mm.
- A candidate must pass the following track isolation requirement:
  - When investigating a cone of size $\Delta R = \sqrt{(\Delta\phi)^2 + (\Delta\eta)^2} = 0.3$ around an muon candidate, if the sum of transverse momenta of tracks which are associated to the primary vertex is larger than 400 MeV, it is required that this sum of transverse momenta would be less than 12% of the electron p_T[3].

4.5.5 Missing Transverse Energy

The reconstruction algorithm for missing transverse energy uses the energy deposition in the calorimeter cells. If the cells are associated with physics objects (electrons, photons, jets and muons), the energy is calibrated respectively, otherwise, when cells are not associated with any object, the energy is weighted to take pile-up effects into account.

4.5.6 Overlap Removal

The Overlap Removal procedure aims to remove duplication of a particular object in more than one baseline particle collection. This procedure is common to all the SUSY electroweak production analyses. The following steps which describe the procedure, are applied consecutively in the order they are presented here.

1. $\Delta R(e_1, e_2) \geq 0.05$: If any two baseline electrons (e_1 and e_2) lie within a distance $\Delta R < 0.05$ of each other, the electron with the lower cluster energy E_T is rejected to avoid electrons from photon conversion.

2. $\Delta R(e, j) \geq 0.2$: If the distance between a baseline electron (e) and a jet (j) is smaller than 0.2, the jet is rejected to avoid object duplication.

[3]Marked as $p_T cone30/p_T < 0.12$ in Table 4.2. $p_T cone30$ denotes the sum of the p_T within a cone of size $\Delta R = 0.3$.

Taus			
	Baseline	Signal	
Cut	Value / Description	Value / Description	
algorithm	cluster seeded	cluster seeded	
p_T	$p_T > 20$ GeV	$p_T > 20$ GeV	
η-acceptance	$\|\eta\| < 2.47$, $\|\eta_{leadTrack}\| < 2.47$	$\|\eta\| < 2.47$, $\|\eta_{leadTrack}\| < 2.47$	
n-prongs	n-prongs = 1 or 3	n-prongs = 1 or 3	
charge	$\|q\| = 1$	$\|q\| = 1$	
quality	loose i.e. jet BDT loose, electron BDT loose (1-prong taus only)	tight i.e. jet BDT tight, electron BDT loose (1-prong taus only), muon veto	
Electrons			
	Baseline	Signal	
Cut	Value / Description	Value / Description	
algorithm	`egamma`	`egamma`	
p_T	$p_T > 10$ GeV	$p_T > 10$ GeV	
η-acceptance	$\|\eta\| < 2.47$	$\|\eta\| < 2.47$	
quality	medium++	tight++	
isolation	-	$p_T cone30/p_T < 0.16$ $E_T cone30/p_T < 0.18$	
tracking cuts	-	various	
Muons			
	Baseline	Signal	
Cut	Value / Description	Value / Description	
algorithm	`STACO` (combined and segment-tagged)	`STACO` (combined and segment-tagged)	
p_T	$p_T > 10$ GeV	$p_T > 10$ GeV	
η-acceptance	$\|\eta\| < 2.4$	$\|\eta\| < 2.4$	
isolation	-	$p_T cone30/p_T < 0.12$	
tracking cuts	various	various	
Jets			
	Baseline	Signal	
		`L30`	`B20`	`F30`
Cut	Value / Description	Value / Description	
algorithm	anti-k_t ($R = 0.4$)	anti-k_t ($R = 0.4$)	
p_T	$p_T > 20$ GeV	> 30 GeV	> 20 GeV	> 30 GeV
η-acceptance	-	$\|\eta\| < 2.4$	$\|\eta\| < 2.4$	$\|\eta\| > 2.4$, $\|\eta\| < 4.5$
JVF	-	$\|JVF\| > 0$ if $p_T < 50$ GeV	-	-
b-tag	-	not b-tagged	b-tagged	-

Table 4.2: Summary of all Baseline and Signal Object Selection Criteria. More Details are given in the text.

3. $\Delta R(e/\mu, \tau) \geq 0.2$: If the distance between a baseline electron/muon (e/μ) and baseline tau (τ) is smaller than 0.2, then the tau is rejected to avoid object duplication, since the electron/muon reconstruction is more precise.

4. $\Delta R(j, e/\mu) \geq 0.4$: If the distance between a remaining jet (j) and a baseline electron/muon (e/μ) still smaller than 0.4, then the baseline electron/muon is rejected to avoid leptons from a semileptonic c- or b-decay inside a jet.

5. $\Delta R(e, \mu) \geq 0.01$: If a baseline electron and a baseline muon lie within a distance of $\Delta R < 0.01$, then both the electron and the muon are rejected due to the difficulty to recognize the object.

6. $\Delta R(\mu_1, \mu_2) \geq 0.05$: If any two baseline muons (μ_1 and μ_2) lie within a distance of $\Delta R < 0.05$, both muons are rejected due to the difficulty to determine the muon position.

7. $m(e_1^{\pm}, e_2^{\mp}/\mu_1^{\pm}, \mu_2^{\mp}) \geq 12$ GeV: To remove low mass resonances, if the invariant mass of any baseline electron or muon pair with opposite sign ($e_1^{\pm}$ and $e_2^{\mp}/\mu_1^{\pm}$ and $\mu_2^{\mp}$) is less than 12 GeV, then both electrons/muons are rejected.

4.5.7 Event "Quality" Criteria

Events considered in this analysis are based on "event quality" requirements which include requirements on the jet quality, the number of tracks associated with the primary vertex as well as the quality of muon signatures and the presence of cosmic muons coinciding with the collision event. A summary of the "quality" selections is presented in Table 4.3.

4.5.8 Trigger Selection

In this thesis the single-lepton trigger is used. This trigger requires identification of one light lepton with transverse momentum larger than 25 GeV, in each selected event.

4.5.9 Tau Scale Factors

In MC processes, every event is scaled via scale factors depending on object quantities, such as tau p_T, η, BDT working points, etc., and on the true nature of the reconstructed tau according to object origin records from MC. The scale factors are applied in order to correct for differences in tau reconstruction in MC with respect to data.

Cut	Description
GRL	Events in data must pass requirements on data quality.
Tile Trip	Events in data must be without corrupted data from the Tile Calorimeter.
Incomplete TTC Veto	Events in data must not be incomplete as a result of a Timing, Trigger and Control (TTC) restart for detector recovery during data-taking.
LAr&Tile Error	Events in data must report no error after LAr and Tile quality assessment.
Tile Hot Spot	Events in data period B1-B2 must not contain jets with a large jet-energy fraction in the second Tile layer pointing to the hot Tile Calorimeter cell ($-0.2 < \eta < -0.1$ and $2.65 < \phi < 2.75$).
Jet Cleaning	Events must not contain a jet which failed the jet quality selection.
Primary Vertex	The primary vertex in the event must be associated with at least 5 tracks.
Bad Muon Veto	Events must not contain a muon which failed the bad muon criteria.
Cosmic Muon Veto	All muons in the event must pass the cosmic muon rejection cuts.

Table 4.3: Event "quality" criteria. Detailed list of the cuts applied at the event selection level.

Chapter 5

Origin of Leptons in SM Background Processes

The use of Monte Carlo samples with ATLAS reconstruction algorithms provides the opportunity to test the final state objects via the 'truth' information stored in MC. It contains the real origin for each object in the simulation. In this analysis, the significant objects in the final state are leptons. This chapter presents studies of the 'truth' origin of reconstructed signal leptons in the studied final state for each SM background[1].
The final state distinguishes between two channels:

- TE Channel - represents the final state with one hadronically decaying tau and one tau which decays into an electron and neutrinos.
- TM Channel - represents the final state with one hadronically decaying tau and one tau which decays into a muon and neutrinos.

The possible origins of the reconstructed leptons are split into seven categories:

1. Prompt lepton : real lepton (true lepton with the same flavour).
2. Conversion (CON) : electron from photon conversion.
3. Light flavour (LF) : light flavour hadron reconstructed as lepton.
4. Heavy flavour (HF) : heavy flavour jet reconstructed as lepton or semi-leptonic heavy quark decay.
5. Electron : prompt electron (this option is relevant only for taus, when a prompt electron is reconstructed as tau).
6. Muon : prompt muon (this option is relevant only for taus, when a prompt muon is reconstructed as tau).
7. Unknown : the reconstructed lepton does not match any other category.

Reconstructed leptons which match same flavour prompt leptons are specified as 'real leptons', while leptons from other origins are specified as 'fake leptons'.

[1]Except for multi-jet production which is estimated from data.

5.1 W+Jets Processes

The origin of the leptons in the W+jets processes is presented in Figure 5.1. In the TE channel the dominant decay is $W \to e\nu$, while the TM channel is dominated by the $W \to \mu\nu$ decay. Figures 5.1(a) and 5.1(b) show the distribution of the origin of the electrons and the muons in the TE and TM channels (i.e. the light leptons distributions). These figures present high probability ($> 99\%$) that a reconstructed light lepton matches a prompted light lepton. Contribution from $W \to \tau\nu$ occurred in both channels and arises from leptonic tau decay products.

Figures 5.1(c) and 5.1(d) present the distributions for the origin of the reconstructed taus in the TE and TM channels, respectively. In both channels most of the taus ($> 99\%$) are fake taus, mostly being mis-identified light flavour jets with additional dominant contributions from conversion and heavy flavour.

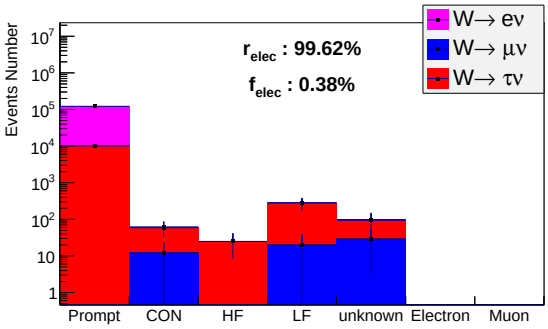

(a) Electron origins.

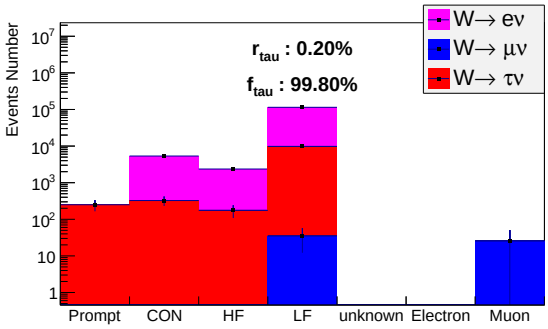

(c) Tau origins - TE channel.

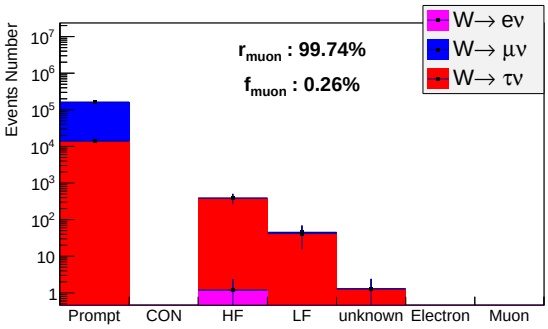

(b) Muon origins.

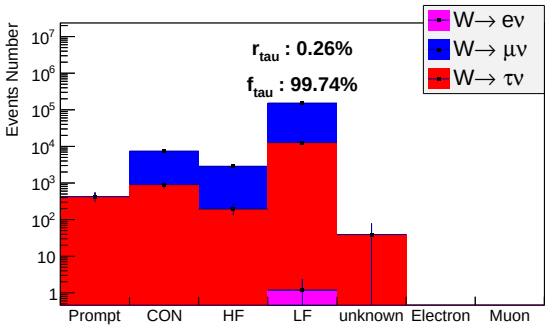

(d) Tau origins - TM channel.

Figure 5.1: Distributions for the origin of the reconstructed leptons in the W+jets processes. 'r_{lepton}' and 'f_{lepton}' show the percentage of real and fake leptons, respectively.

5.2 Z+jets Processes

Leptonic Z boson decays have been investigated. In general, all the reconstructed leptons in these processes has probability higher than 84% to match real leptons. The dominant decay in the TE and the TM channels is $Z \to \tau\tau$, as can be seen in Figure 5.2, where one hadronically decaying tau and one light lepton (originating from a leptonic tau) are detected. In this case, both of the reconstructed leptons have a high probability to be real. In the other decays, $Z \to ee$ and $Z \to \mu\mu$, the selected events include a real light lepton and a fake tau. In the TE channel fake taus mostly arise from mis-identified light flavour jets as well as from electrons (Figure 5.2(c)). In the TM channel most of the fake taus originate from light flavour jets, however other dominant contribution arises from mis-identified muons (Figure 5.2(d)).

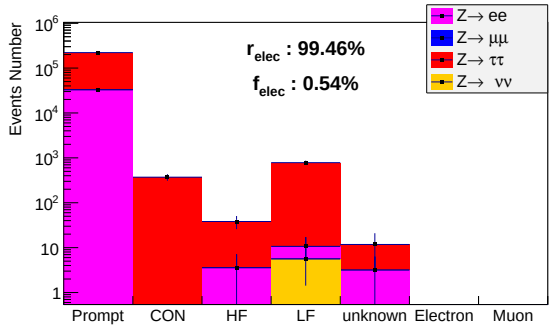

(a) Electron origins.

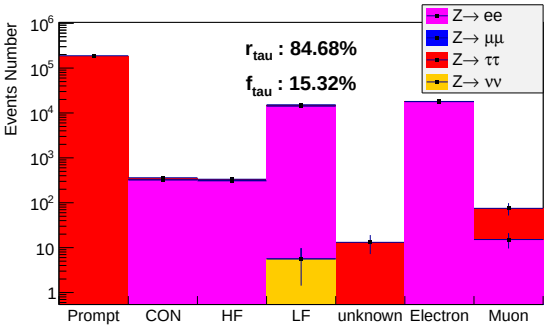

(c) Tau origins - TE channel.

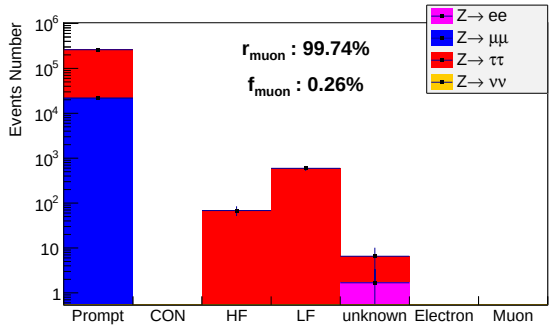

(b) Muon origins.

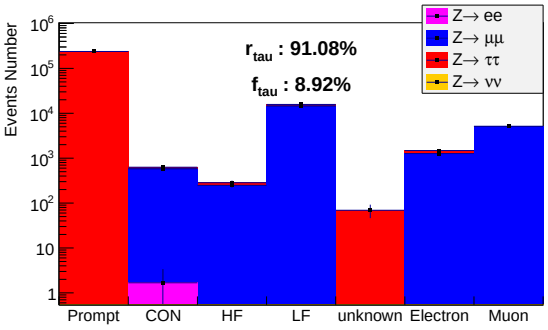

(d) Tau origins - TM channel.

Figure 5.2: Distributions for the origin of the reconstructed leptons in the Z+Jets processes. 'r_{lepton}' and 'f_{lepton}' show the percentage of real and fake leptons, respectively.

5.3 Diboson Processes

For the diboson processes all of the reconstructed objects have a probability higher than 93% for being prompt leptons. The highest probabilities ($> 99\%$) are for light leptons, as Figures 5.3(a) and 5.3(b) show. In both channels some fake taus are present due to light flavour jets and electrons which are mis-identified as taus. This can be seen in Figures 5.3(c) and 5.3(d).

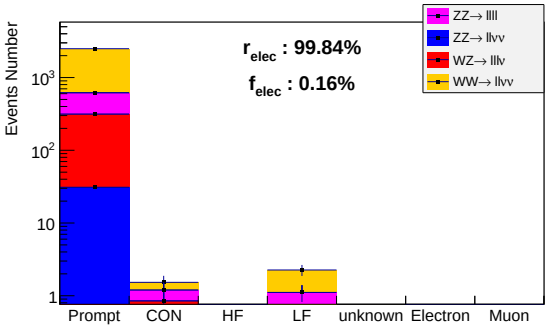

(a) Electron origins.

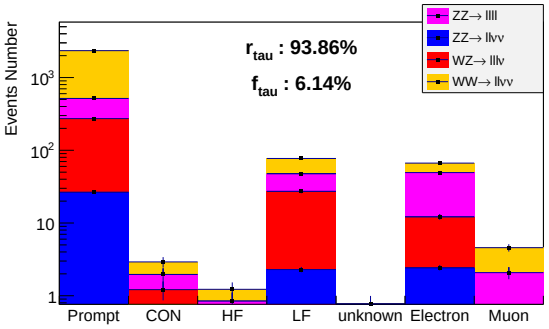

(c) Tau origins - TE channel.

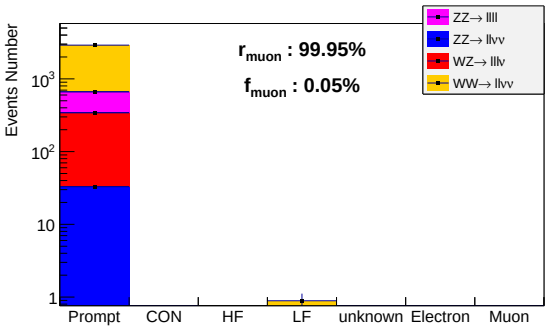

(b) Muon origins.

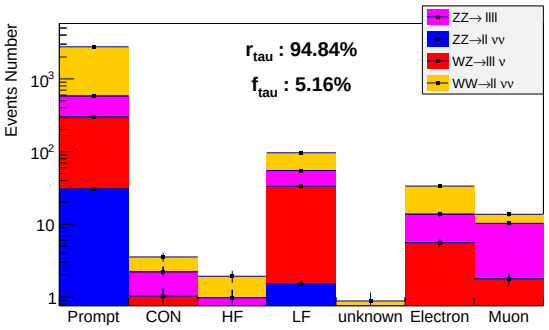

(d) Tau origins - TM channel.

Figure 5.3: Distributions for the origin of the reconstructed leptons in the diboson processes. 'r_{lepton}' and 'f_{lepton}' show the percentage of real and fake leptons, respectively.

5.4 $t\bar{t}$ Processes

The $t\bar{t}$ processes decay into $b\bar{b}$ and W^+W^- pairs, where the W bosons can decay hadronically or leptonically. Figure 5.4 shows the distributions for the origin of reconstructed leptons in $t\bar{t}$ processes. The dominant decays in this final state are decays where one top quark decays into light leptons and the second decays hadronically, which is compatible with the cross sections for these decays. The reconstructed light leptons are real with high probability ($> 99\%$), while only $\sim 75\%$ of the taus are real.

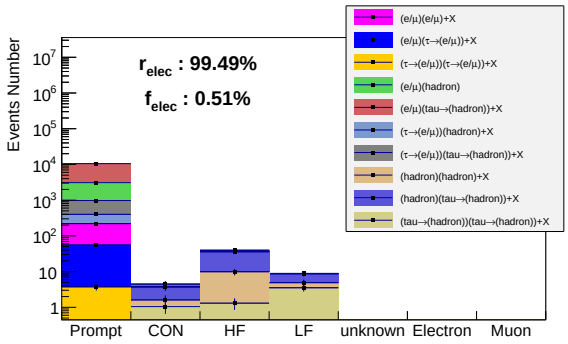

(a) Electron origins.

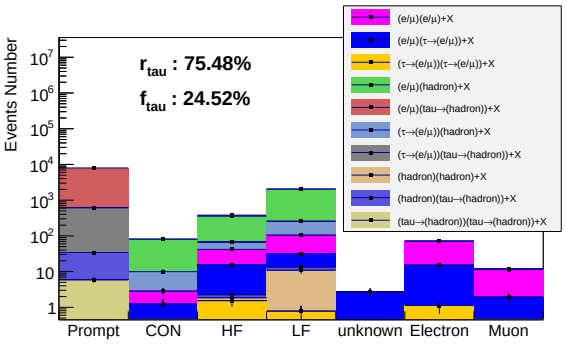

(c) Tau origins - TE channel.

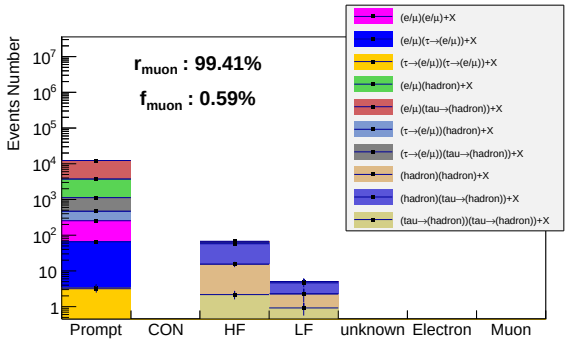

(b) Muon origins.

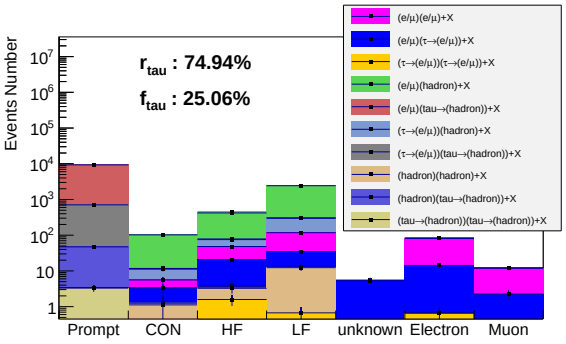

(d) Tau origins - TM channel.

Figure 5.4: Distributions for the origin of the reconstructed leptons in the $t\bar{t}$ processes. The different WW decays are presented with or without intermediate taus; the X indicates the b hadrons and the undetected particles. 'r_{lepton}' and 'f_{lepton}' show the percentage of real and fake leptons, respectively.

5.5 Summary

In the data records all background processes are simultaneously present. In order to simulate the complete picture (without multi-jet contribution) in this final state, a combination of all the above SM backgrounds with respect to their cross sections is presented in Figure 5.5. The main background processes are W+jets and Z+jets processes due to their large cross sections. Figures 5.5(a) and 5.5(b) show the distributions for the origin of the reconstructed electrons in TE channel and reconstructed muons in TM channel, respectively. Both channels present a good reconstruction of the light leptons, with probabilities higher than 99% for reconstructed light leptons to match prompt leptons.
Nevertheless in the tau reconstruction process, other objects can be mis-identified as taus. The fraction of fake taus is larger than 43% in each channel, as can be seen in Figures 5.5(c) and 5.5(d). The majority of fake taus originates from mis-identified light flavour jets, mostly reconstructed in W+jets processes, where the other dominant contributions originate from conversion and heavy flavour in W+jets processes or from mis-identified electrons and muons in Z+jets processes.
The difficulty in tau reconstruction process is caused by the short lifetime of the tau lepton, in contrast to the lifetime of the other leptons. Therefore we can only detect the products of the tau decay. In hadronic decays a mixture of neutral and charged π-mesons are produced. The charged ones can be detected in the Inner Detector and in the Hadronic Calorimeter, while the neutral pions are detected in the Electromagnetic Calorimeter. The combination is done via the reconstruction algorithm, which was explained in section 4.5.2. Altogether, the reconstruction procedure for hadronically decaying taus becomes very complicated.

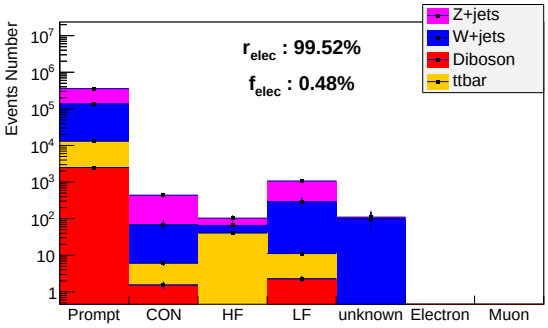

(a) Electron origins.

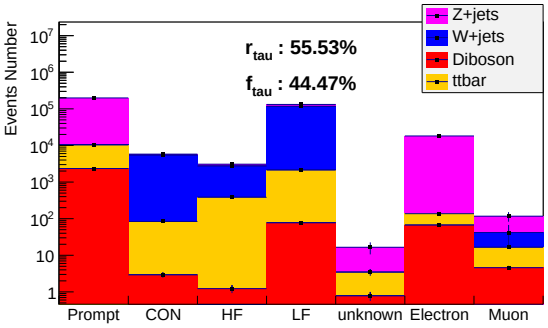

(c) Tau origins - TE channel.

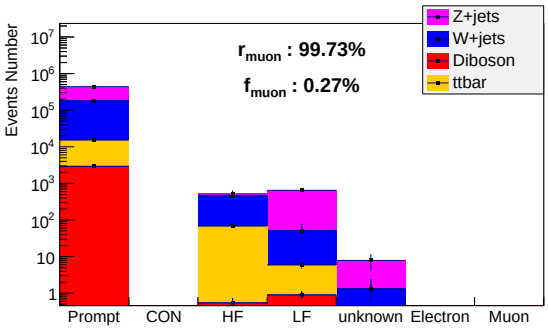

(b) Muon origins.

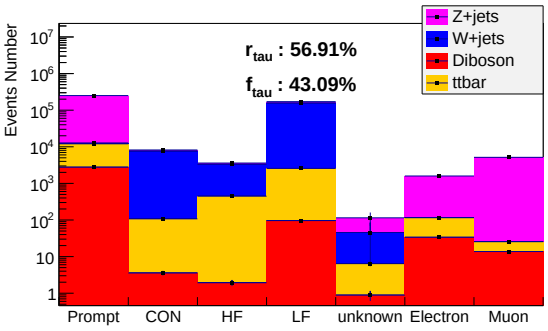

(d) Tau origins - TM channel.

Figure 5.5: Distributions for the origin of the reconstructed leptons in all SM background processes (without multi-jet production) in the final state with one hadronically decaying tau and leptonically decaying tau. The labels 'r_{lepton}' and 'f_{lepton}' represent the percentage of real and fake leptons, respectively.

Chapter 6

Tau-Identification Efficiencies

In Chapter 5, the selected hadronically decaying taus are separated into prompt real taus and fake taus. We see that more than 43% of the taus which pass the event selection (Section 4.5) are mis-identified objects.
This chapter presents measurements of real and fake efficiencies. Two sets of tau selection criteria have been defined, "loose" selection and "tight" selection. The real efficiency (r) is the probability of a real, prompt loose tau to pass the tight selection criteria. The fake efficiency (f) is the probability of a fake, non-prompt loose tau to pass the tight selection criteria.

$$r = \frac{N_{real}^{tight}}{N_{real}^{loose}} \qquad\qquad f = \frac{N_{fake}^{tight}}{N_{fake}^{loose}} \tag{6.1}$$

All the measurements in this chapter are in the TM channel. We define loose taus as baseline taus and tight taus as signal taus, where the additional muon is a signal muon which has fired the single isolated muon trigger. The definition for baseline and signal leptons, as well as the trigger selection are detailed in Section 4.5.
The uncertainties on both data and MC are only statistical, no systematic uncertainties have been taken into account.

6.1 Estimation of Real and Fake Efficiencies from Monte Carlo Samples

Monte Carlo (MC) samples provide the MC truth information which can be used to measure the efficiencies directly. The following estimation includes events which contain exactly one baseline tau and one signal muon which has fired the single isolated muon trigger with $p_T \geqslant 25$ GeV. The efficiencies were measured as a function of tau p_T, η and number of prongs.
The measurements are presented in Figures 6.1 and 6.2. The real efficiencies are similar for Z+jets, diboson and $t\bar{t}$ processes. As for the W+jets processes, the measurement of real taus in this background has low statistics. In Figure 6.1, we see a slightly higher fake efficiency in Z+jets processes compared to other processes. We can assume that this difference originated from mis-identified muons in the Z+jets production, which are not dominant in the other processes.
Average values of the efficiencies were calculated using the total number of selected tight taus (1-prong or 3-prong taus) over the total number of selected loose taus

(1-prong or 3-prong taus) with respect to the statistical uncertainties. The average values of the real efficiency are 0.537±0.001 for 1-prong taus and 0.568±0.002 for 3-prong taus. Average values for the fake efficiency are 0.220±0.002 for 1-prong taus and 0.157±0.003 for 3-prong taus.

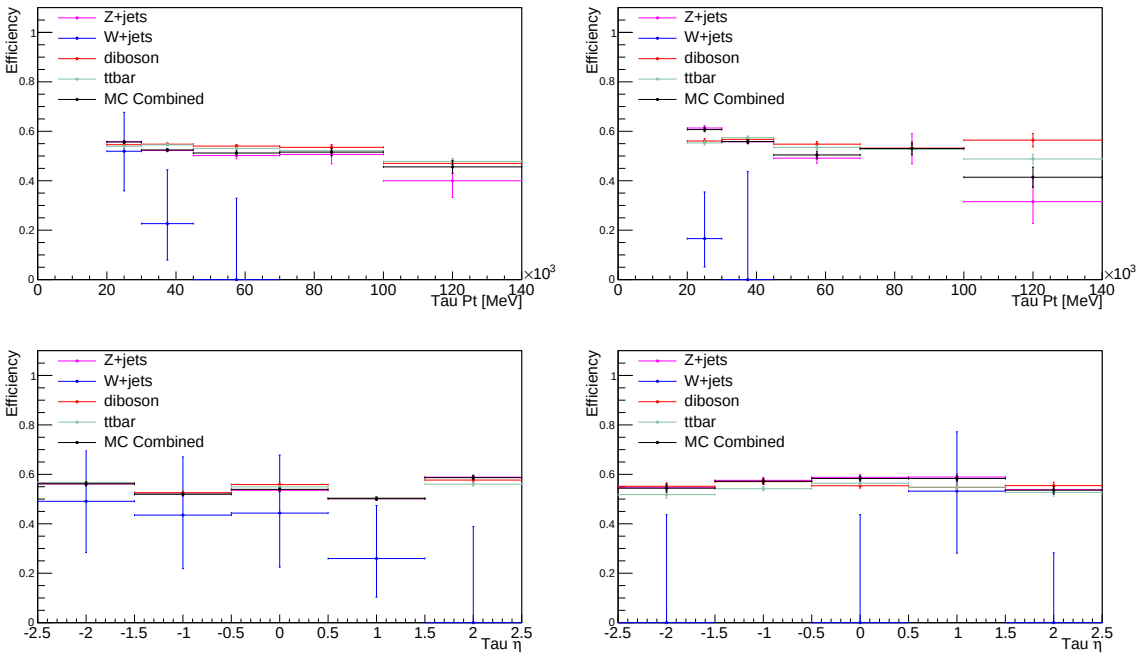

Figure 6.1: Real efficiencies for 1-prong taus (left) and 3-prong taus (right) as a function of tau p_T and η as measured in MC truth for TM events after trigger decision. The uncertainties are statistical uncertainties.

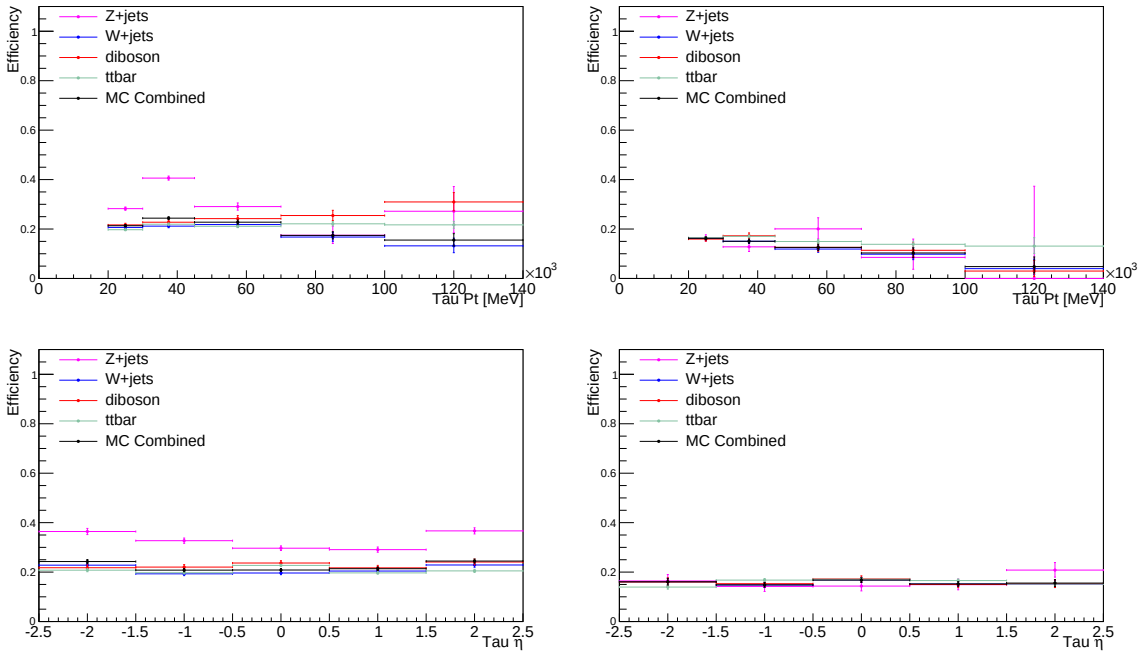

Figure 6.2: Fake efficiencies for of 1-prong taus (left) and 3-prong taus (right) as a function of tau p_T and η as measured in MC truth for TM events after trigger decision. The uncertainties are statistical uncertainties.

6.2 Measurements in Data

Data samples are not allowing direct distinction between real and fake taus. Therefore the efficiencies are taken from the MC estimations and corrected via scale factors (SF's). The scale factors are assumed to be independent of the process, namely the same (real or fake) scale factor is applied to (real or fake) efficiencies of different SM processes. The scale factor is defined as the ratio of the efficiency measured in data over the efficiency estimated via MC.

$$SF_{fake} = \frac{f_{data}}{f_{MC}} \qquad SF_{real} = \frac{r_{data}}{r_{MC}} \tag{6.2}$$

The SF measurements are done in Control Regions (CR's) with high probability to find real or fake taus. The CR's were chosen according to the studies in the last chapter. In Figure 5.5 it can be seen that Z+jets processes produce most of the real taus. Therefore the real CR is defined to select events with $Z \longrightarrow \tau(\rightarrow hadron)\tau(\rightarrow \mu)$ process. This CR is indicated as the ZCR.
W+jets is the SM background with the largest number of fake taus, in particular from light flavor jets. A W+jets enriched region is defined as the fake CR and indicated as WCR.

6.2.1 Multi-jet Background

The multi-jet background is an important SM background in this final state. Nevertheless, it is very difficult to simulate it using MC samples, due to its large cross section and the low probability for events with two reconstructed taus. Hence, while the other SM processes are estimated directly from MC, the multi-jet contribution is estimated from data.
The estimation is done within same-sign (SS) CRs, i.e. CRs in data which satisfy the same requirements as the control regions but select events where the tau and the muon have the same charge (same sign). The number of multi-jet events is estimated by subtracting the MC events (all SM productions except to multi-jet) from the data counts.

$$N^{OS}_{multi-jet} = N^{SS}_{multi-jet} = N^{SS}_{data} - N^{SS}_{MC(non-multi-jet)} \tag{6.3}$$

The method relies on the fact that in the multi-jet background the ratio of SS and opposite-sign (OS) events is close to unity, whilst a significant difference from unity is expected from other SM processes.
In this analysis we discriminate between multi-jet background and fake background. The multi-jet production contains events with two fake leptons, whereas fake background refers to events with a fake hadronically tau and a prompt muon.

6.2.2 Z+jets Control Region

Within the Z+jets Control Region (ZCR) events with $Z \longrightarrow \tau(\rightarrow hadron)\tau(\rightarrow \mu)$ process are selected. These events provide a large contribution to the total number of events with real taus in this analysis. The ZCR is defined by the following cuts:

- The event contains one tau and one muon with OS (TM channel).
- The muon is required to have fired the single isolated muon trigger with $p_T \geqslant 25$ GeV.
- The invariant mass of selected muon and tau, $m_{\tau\mu}$ is required to be within a range close to the Z boson mass (which was measured to be 91.1876±0.0021 GeV according to [6]): $40 < m_{\tau\mu} < 100$ GeV.
- The sum of the muon and tau transverse masses is required to be lower than 80 GeV: $m^{\tau}_T + m^{\mu}_T < 80$ GeV, where the transverse mass is defined by $m_T = \sqrt{2 \cdot E^{miss}_T \cdot p_T(lepton) \cdot (1 - \cos\Delta\phi(\vec{E}^{miss}_T, \vec{p}_T(lepton)))}$.
- The difference between the tau and muon azimuthal angles ϕ must be larger than 2.4: $\Delta\phi_{\tau\mu} > 2.4$.
- Events which include b-tagged jets are vetoed.

Figures 6.3, 6.4 and 6.5 present the distributions of characteristic properties of ZCR: the sum of transverse masses, the invariant mass and the $\Delta\phi$ of the tau and the muon. The agreement between data and SM background is not covered by the statistical uncertainties range. Systematic uncertainties are not included in this analysis, however they have been estimated by a similar analysis to be in the order of 20% [43]. If we consider statistical and systematic uncertainties, the data measurements are compatible with MC estimations.

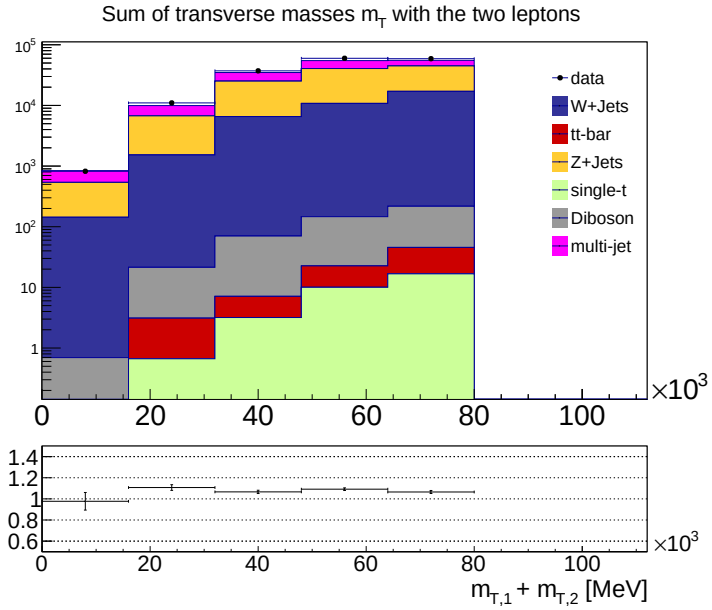

Figure 6.3: Distribution of the sum of lepton transverse masses in the SM processes and in data within ZCR. The uncertainties are statistical uncertainties.

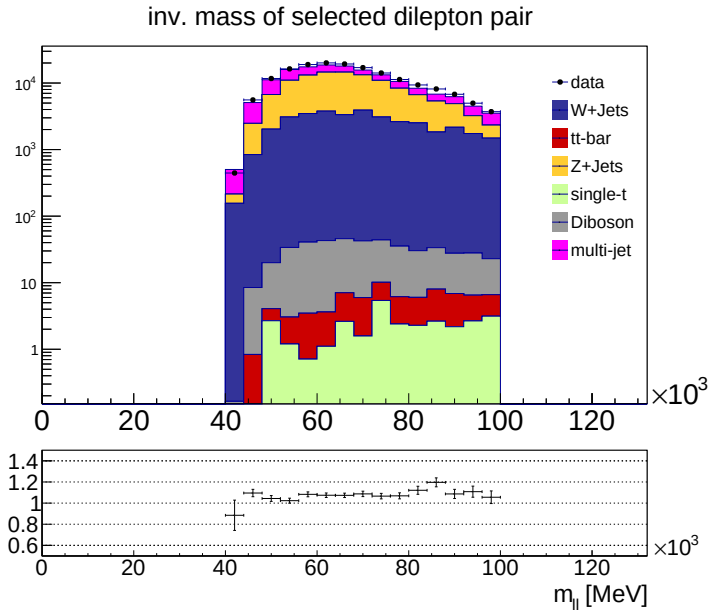

Figure 6.4: Distribution of the invariant mass of leptons in the SM processes and in data within ZCR. The uncertainties are statistical uncertainties.

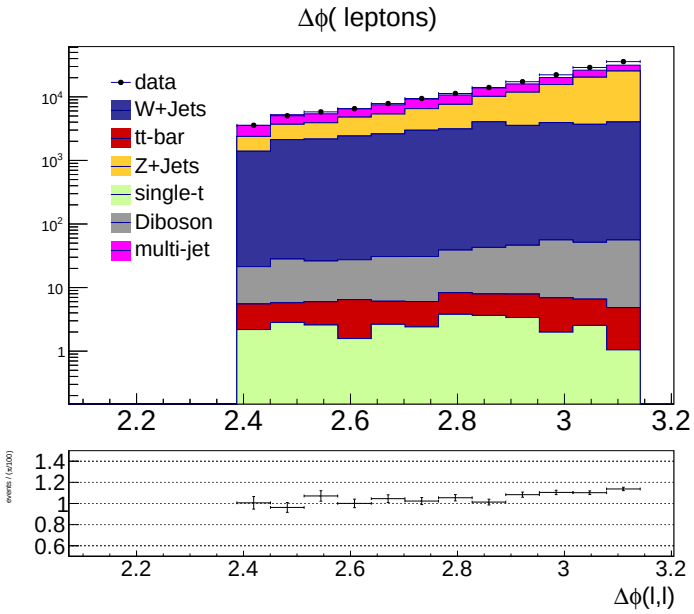

Figure 6.5: Distribution of $\Delta\phi_{\tau\mu}$ between the leptons in the SM processes and in data within ZCR. The uncertainties are statistical uncertainties.

When choosing a control region, an important parameter is purity. Purity is derived from the MC and multi-jet estimations. It is defined as the number of events in the desirable production over the number of events from all SM estimations within the CR. In ZCR purity is defined as

$$\text{Purity}^{ZCR} = \frac{N^{Z+jets}}{N^{SM\ processes}} \tag{6.4}$$

High purity indicates good event selection, nevertheless the statistics must be reasonable. Table 6.1 shows the number of events in ZCR when the full 20.3 fb^{-1} dataset is used. All SM processes except for multi-jet processes are taken from the MC samples. Multi-jet contribution is estimated as described in Section 6.2.1. The purity achieved in this CR is 52%.

	Events number
Z+jets	81683±571
Multi-jet	38058±717
W+jets	35609±890
Diboson	378±6
tt-bar	48±3
Single-t	31±4
SM total	155806±1278
Data	167805 ±410
Purity	0.5242±0.0006

Table 6.1: The number of events in ZCR from the SM processes and data; ZCR purity. The uncertainties are statistical uncertainties.

Figures 6.6 and 6.7 illustrate the distributions of tau p_T and η (without the dependence on the number of prongs in the hadronic tau decay) in ZCR separated for different processes. Again we can see that within the statistical uncertainties range the agreement between data and MC is not good, but with additional systematic uncertainties of 20% the agreement would improve.

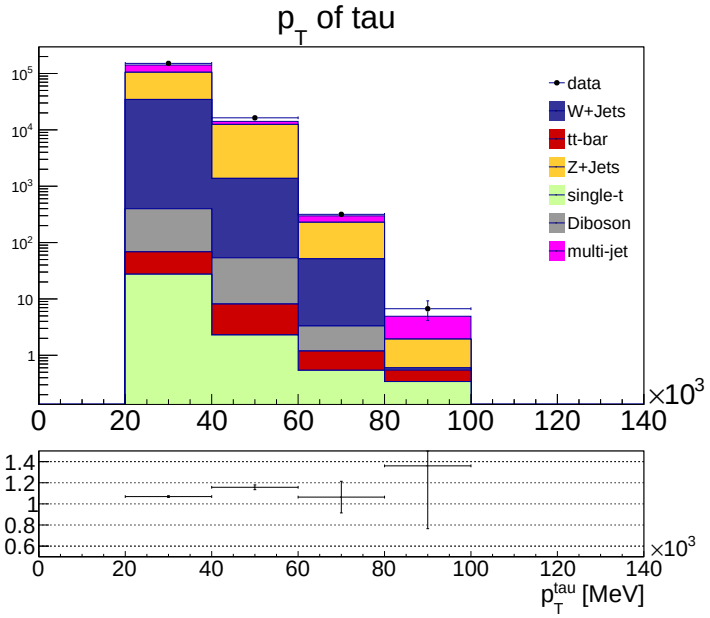

Figure 6.6: Distribution of tau p_T in the SM processes and in data within ZCR. The uncertainties are statistical uncertainties.

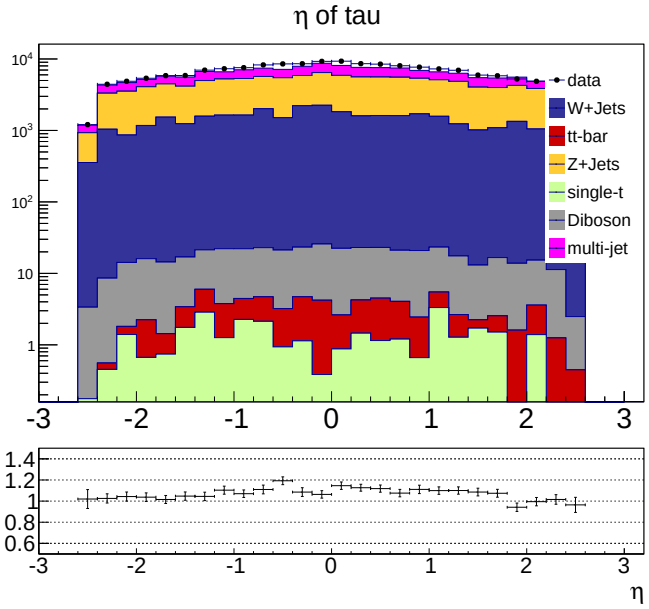

Figure 6.7: Distribution of tau η in the SM processes and in data within ZCR. The uncertainties are statistical uncertainties.

Scale Factors for Real Efficiencies

Defining ZCR as a region which mainly selects events with real taus, enables measurements of real efficiencies in data and MC samples. The efficiency measurements in MC use of the truth information to select only real taus. However, since multi-jet background is not estimated by MC samples, we must subtract its estimation from the data measurements. In addition we subtract the MC fake background. These measurements are described in the form:

$$r_{MC} = \frac{N^{tight}_{MCreal}}{N^{loose}_{MCreal}} \tag{6.5}$$

$$r_{data} = \frac{N^{tight}_{data} - N^{tight}_{multi-jet} - N^{tight}_{MCfake}}{N^{loose}_{data} - N^{loose}_{multi-jet} - N^{loose}_{MCfake}} \tag{6.6}$$

The efficiencies are parametrized by the tau p_T, η and the number of prongs; the measurements are presented in Figure 6.8. Due to the Z boson mass, we can see measurements with low statistics in the higher p_T range.
The average values of the efficiencies were calculated using formulas 6.5 and 6.6 only as a function of the number of prongs and taking into account the statistical uncertainties. For 1-prong taus the average real efficiency from data is 0.419±0.002, while the measurement from MC is 0.550±0.002. A similar difference is noticeable in the 3-prong case with measurements of 0.412±0.002 in data and 0.600±0.002 in MC.
As shown in Figure 6.8, the scale factors vary with the parameters and therefore are not considered to be constants. For each p_T or η value a different scale factor is applied and different error is taken into account. In addition, we can notice that the efficiencies as a function of the tau p_T have different shapes. This difference will be investigated in further studies.
The average values of the scale factors, which are based on the average values of the efficiencies, are 0.761±0.001 for 1-prong taus and 0.686±0.001 for 3-prong taus.

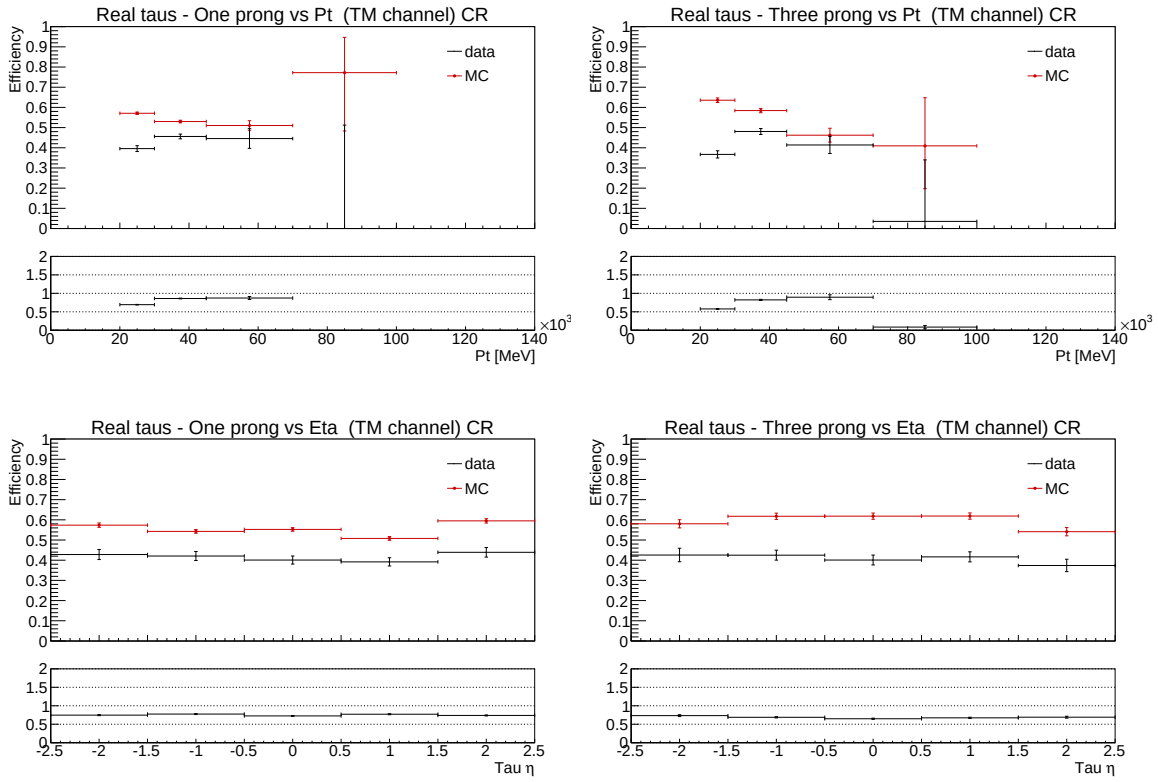

Figure 6.8: Real efficiencies of 1-prong taus (left) and 3-prong taus (right) as a function of tau p_T and η, as measured in ZCR with the use of MC truth information. The uncertainties are statistical uncertainties.

6.2.3 W+jets Control Region

The W+jets Control Region (WCR) selects events with $W \to \mu\nu$ process. These events pass the event selection with a real muon and a fake tau, thus contribute to the fake background. The WCR is defined by the following cuts:

- The event contains one tau and one muon with OS (TM channel).
- The muon is required to have fired the single isolated muon trigger with $p_T \geqslant 25$ GeV.
- $\sum \cos(\Delta\phi) = \cos(\Delta\phi(E_T^{miss}, \mu) + \cos(\Delta\phi(E_T^{miss}, \tau)) \leqslant -0.15$.
- Events with b-tagged jets are vetoed.
- The distance ΔR between the muon and the tau must be larger than 0.3: $\Delta R = \sqrt{(\Delta\phi)^2 + (\Delta\eta)^2} > 0.3$.
- The event must have missing transverse energy greater than 40 GeV: $E_T^{miss} > 40$ GeV.

Figures 6.9 and 6.10 present comparison plots between data and SM processes for WCR properties. We can see good agreement between the data and the SM processes in respect to the statistical uncertainties.

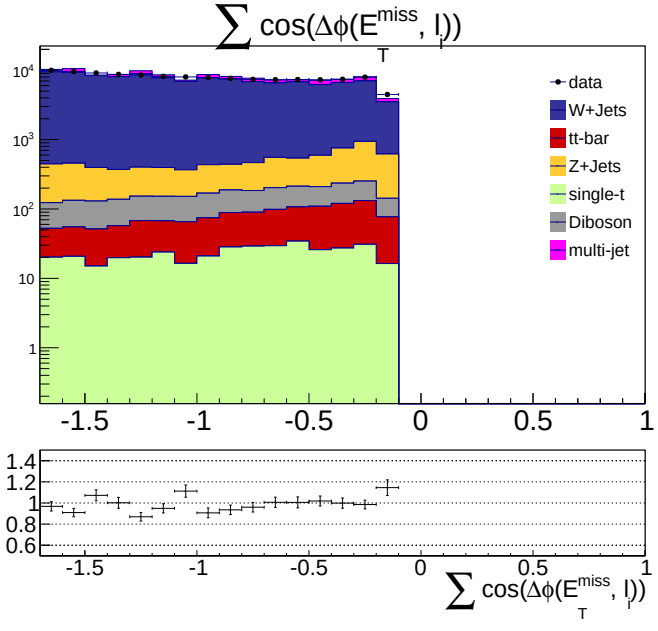

Figure 6.9: Distribution of $\sum \cos(\Delta\phi)$ in the SM processes and in data within WCR. The uncertainties are statistical uncertainties.

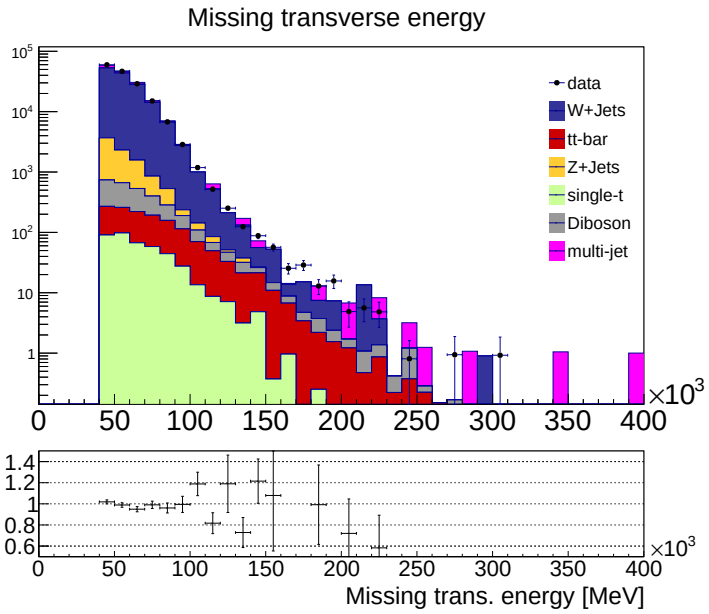

Figure 6.10: Distribution of missing transverse energy in the SM processes and in data within WCR. The uncertainties are statistical uncertainties.

The purity in WCR is defined as

$$\text{Purity}^{WCR} = \frac{N^{W+jets}}{N^{SM\ processes}} \tag{6.7}$$

The contributions from the different SM processes in comparison with data are detailed in Table 6.2. The WCR control region was successfully optimized to produce high purity of 86% as well as large statistics.

Figures 6.11 and 6.12 present the p_T and η distributions of the tau (without the dependence on the number of prongs in the hadronic tau decay) within the WCR, separated for the different SM backgrounds in comparison to measurements from data. Again, we see a good agreement between data and the SM background estimation in respect to the statistical uncertainties.

	Events number
W+jets	140979±1776
Multi-jet	13001±1410
Z+jets	6439±152
Diboson	1692±14
tt-bar	1014±14
Single-t	424±17
SM total	163551±2273
Data	162304±400
Purity	0.861±0.001

Table 6.2: The number of events in WCR from the SM processes and data; WCR purity. The uncertainties are statistical uncertainties.

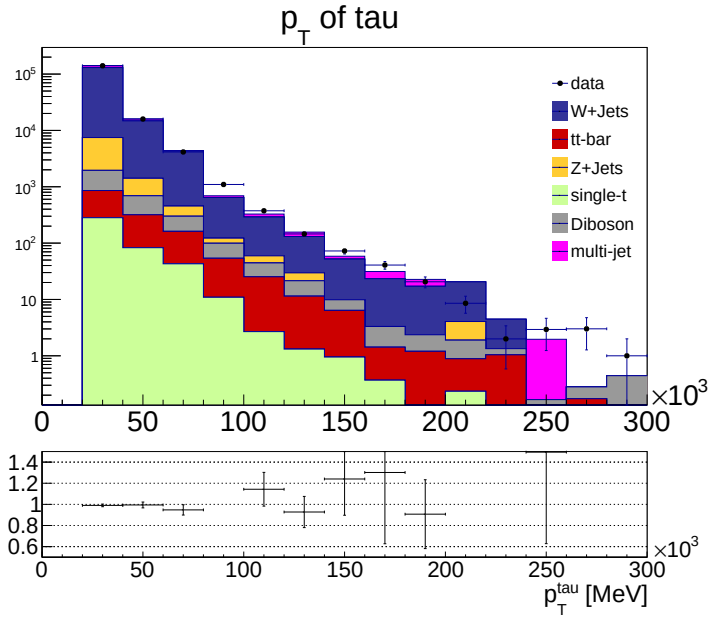

Figure 6.11: Distribution of tau p_T in the SM processes and in data within WCR. The uncertainties are statistical uncertainties.

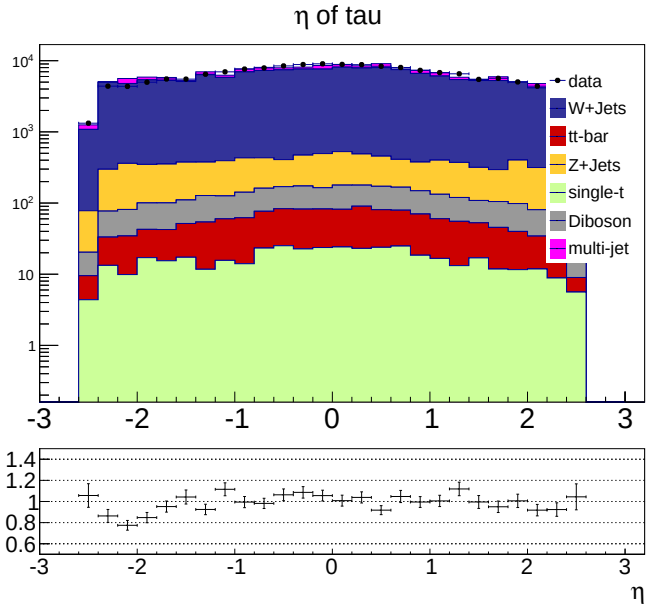

Figure 6.12: Distribution of tau p_T in the SM processes and in data within WCR. The uncertainties are statistical uncertainties.

Scale Factors for Fake Efficiencies

To be consistent with the real efficiency measurements in data, the fake efficiencies are measured according to similar definitions as in the ZCR, using MC truth information and subtracting multi-jet events from the data count. The measurements are described in the form

$$f_{MC} = \frac{N^{tight}_{MCfake}}{N^{loose}_{MCfake}} \tag{6.8}$$

$$f_{data} = \frac{N^{tight}_{data} - N^{tight}_{multi-jet} - N^{tight}_{MCreal}}{N^{loose}_{data} - N^{loose}_{multi-jet} - N^{loose}_{MCreal}} \tag{6.9}$$

and parametrized by tau p_T, η and the number of prongs, where the full 20.3 fb^{-1} dataset was used. The results are presented in Figure 6.13.
The efficiencies were averaged using formulas 6.8 and 6.9 only as a function of the number of prongs and including statistical uncertainties. The average values of the fake efficiencies are 0.179±0.003 in data and 0.191±0.002 in MC for 1-prong taus; and 0.144±0.003 in data and 0.146±0.004 in MC for 3-prong taus.
In Figure 6.13 we can also see that the scale factors vary with the parameters, especially for the p_T dependence. Accordingly the scale factors are implemented as a function of p_T or η. The average values of the scale factors, based on the average values of the efficiencies, are 0.937±0.004 for 1-prong taus and 0.987±0.004 for 3-prong taus.

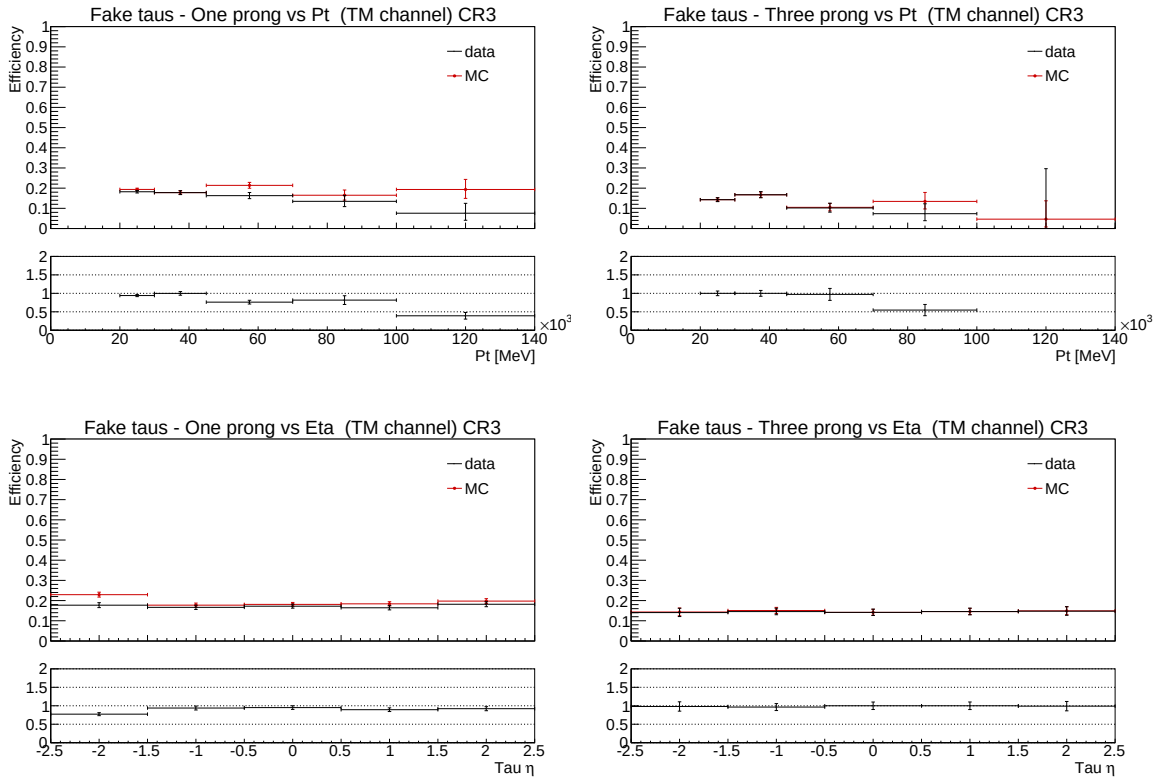

Figure 6.13: Fake efficiencies of 1-prong taus (left) and 3-prong taus (right) as a function tau p_T and η as measured in WCR. The uncertainties are statistical uncertainties.

6.3 Summary

All the average values for the estimations of the real and fake efficiencies, as well as for the scale factors for data/MC correction, are summarized in Table 6.3.
In Section 6.1, we estimated the efficiencies in MC samples with the truth information. We selected events with two opposite sign leptons, one baseline tau and one signal muon which has fired the single isolated muon trigger. This region is marked in the table as 2OSL.
The measurements in data were done in specific control regions.
In Section 6.2.2 we estimated the real efficiencies in data and MC and calculated the real scale factors within the ZCR, a control region which is defined to select events with real taus. In Section 6.2.3 we estimated the fake efficiencies in data and MC and calculated the fake scale factors within the WCR, a control region for selecting events with fake taus.
We saw that the agreement between MC and data is not good in the ZCR within the cover of the statistical uncertainties. However the agreement between MC and data in WCR is good. As a result the real scale factors are low compared with the fake scale factors.

	Region	Dataset	1-prong	3-prong
Real	2OSL	r in MC	0.537±0.001	0.568±0.002
	ZCR	r in MC	0.550±0.002	0.600±0.003
		r in data	0.419±0.002	0.412±0.002
		r scale factor	0.761±0.001	0.686±0.001
Fake	2OSL	f in MC	0.220±0.002	0.157±0.003
	WCR	f in MC	0.191±0.002	0.144±0.003
		f in data	0.179±0.003	0.146±0.004
		f scale factor	0.937±0.005	0.987±0.004

Table 6.3: Summary of the average values of the efficiencies and scale factors.

Chapter 7

The Matrix Method

In this chapter the so-called "Matrix Method" (MM) is being performed and discussed. The Matrix Method is a semi-data driven method which is used to estimate fake background.
The MM requires the same separation for 'loose' and 'tight' selection criteria as it was used to define the efficiencies in Chapter 6. Throughout this chapter, 'loose' or 'tight' event refers to an event with a loose (baseline) or a tight (signal) tau, similarly 'real' or 'fake' event refers to an event with a real or a fake tau.

Within the loose events we can distinguish between events with a fake tau and events with a real tau.

$$N^{loose} = N^{loose}_{real} + N^{loose}_{fake} \tag{7.1}$$

The same distinction can be done within the tight events. It is possible to use the real (r) and fake (f) efficiency definitions as defined in formula 6.1 to describe the number of tight events, N^{tight}, as a linear combination of fake and real loose event.

$$N^{tight} = N^{tight}_{real} + N^{tight}_{fake} = rN^{loose}_{real} + fN^{loose}_{fake} \tag{7.2}$$

From formulas 7.1 and 7.2 it is easy to derive the number of events with a fake signal tau

$$N^{tight}_{fake} = \frac{f}{r-f}(N^{loose}r - N^{tight}) \tag{7.3}$$

Note that the method requires a good separation between the real and fake efficiency.

In general, the Matrix Method efficiencies depend on the object type (tau/light lepton), the production process and the events kinematics (as was shown in Chapter 6).
In order to achieve a good estimation, we construct weighted average efficiencies.
The efficiencies for each process are extracted from MC, corrected for data/MC differences, and then averaged together with a weight representing the relative contribution from each process.

The weighted average fake efficiency and real efficiency for a specific region XR are defined as

$$f_{XR} = \sum_p (f^p \times SF_{fake} \times R_{XR}^{p\ fake}) \tag{7.4}$$

$$r_{XR} = \sum_p (r^p \times SF_{real} \times R_{XR}^{p\ real}) \tag{7.5}$$

where p indicates the production process (in this analysis: Z+jets, W+jets, diboson and $t\bar{t}$). The remaining factors are described below:

The efficiencies, f^p and r^p, are fake and real efficiencies for each SM process p. The efficiencies are defined as the ratio of the number of signal taus over the number of baseline taus for a given process. The tau type (fake/real) is determined from the truth information. In order to accomplish maximum statistics, the efficiencies are measured on events with two leptons, baseline tau and signal muon with OS, which passed the event selection requirements (Section 4.5), whereas the muon is required to have fired the single isolated muon trigger with $p_T \geqslant 25$ GeV.

The scale factors, SF_{fake} and SF_{real}, are correction factors for the fake and real efficiencies to account for the differences between data and MC. They are derived in control regions enriched in fake or real taus. More details on the measurements of the scale factors are provided in Sections 6.2.2 and 6.2.3.

The fractions, $R_{XR}^{p\ fake}$ and $R_{XR}^{p\ real}$, are the fake and real fractions originating from process p in XR. They are used to average the efficiencies. The fractions are measured from MC samples, where the tau type (fake/real) is determined from the truth information.

The weighted average efficiencies are measured as a function of the tau p_T, η and the number of prongs, hence all terms in formulas 7.4 and 7.5 are parametrized as a function of p_T and η for 1 and 3 prong tau decays, respectively.

7.1 Matrix Method in this analysis

In this analysis, an estimation of the tau fake background is done. The SM production with maximum fakes is W+jets production, thus measurements are done with XR = WCR.

The measurements are described below:

- N^{loose} and N^{tight} are determined in WCR as the number of the 'loose' and 'tight' events from the full 20.3 fb^{-1} dataset minus the multi-jet contribution (multi-jet estimation is explained in Section 6.2.1) of 'loose' and 'tight' events.

- $R^{p\ fake}_{WCR}$ and $R^{p\ real}_{WCR}$ are estimated in WCR from MC samples with truth information for each process p.
- The fake and real efficiencies per process, were measured as described in Section 6.1 (in the previous chapter).
- The real and fake SFs were measured in ZCR and WCR, as described in Sections 6.2.2 and 6.2.3.

All the measurements are p_T and η dependent and separated to 1-prong and 3-prong hadronic tau decays. Only statistical uncertainties are taken into account.

7.2 Weighted Average Efficiencies

In order to use the MM to estimate the tau fake background, one must produce the weighted average efficiencies. In Chapter 6 the MC efficiencies and the SF measurements were presented. Fraction measurement is the missing piece.
The real and fake fractions are measured in the investigated region WCR. Figures 7.1 and 7.2 present the results as a function of the tau p_T and number of prongs.

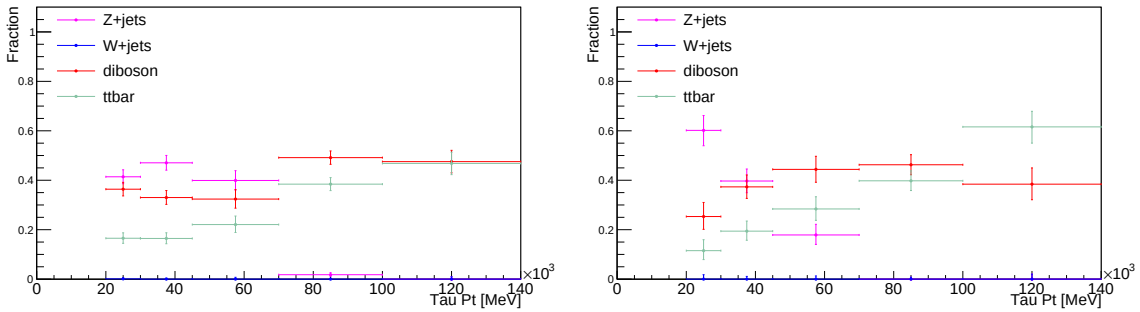

Figure 7.1: Real tau fractions per process as a function of tau p_T in WCR. For 1-prong taus the fractions are shown on the left side and for 3-prong taus on the right side. The uncertainties are statistical.

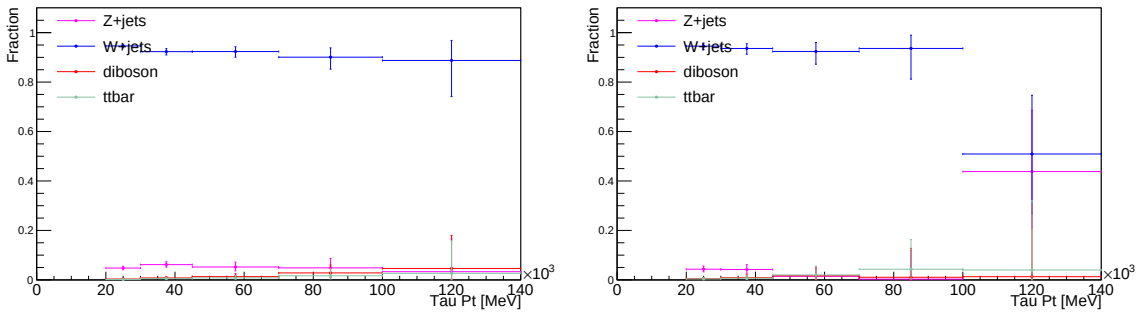

Figure 7.2: Fake tau fractions per process as a function of tau p_T in WCR. For 1-prong taus the fractions are shown on the left side and for 3-prong taus on the right side. The uncertainties are statistical.

Figure 7.1 presents the real fraction for each background. We can see that W+jet background has no real events within the WCR. Most of the real taus originating from Z+jets background in the lower p_T range and from diboson background in the higher p_T range. We should recall that the $\sum \cos(\Delta\phi)$ cut in WCR definitions (Section 6.2.3) is intended to reduce the contribution from the Z+jets background. Figure 7.2 presents the fake fraction per background. It illustrates that most of the fake events within WCR are selected from the W+jets production, as expected.

Using the above measurements together with the measurements presented in Chapter 6, it is possible to construct the real and fake weighted average efficiencies.
Figure 7.3 presents the real weighted average efficiency as a function of tau p_T, η and number of prongs.
Between the p_T range of 70 GeV to 140 GeV, the weighted average real efficiency has very low values. This is caused by the measurement of the real scale factor in the ZCR. This region selects real events with $Z \longrightarrow \tau(\rightarrow hadron)\tau(\rightarrow \mu)$ process, therefore the possible p_T range is limited by the Z boson mass.

The average values for the real efficiency were calculated taking into account statistical errors. For 1-prong taus the average values are 0.40±0.09, and for 3-prong taus the average value is 0.38±0.14. Average values for the fake efficiency were calculated in the same way. 1-prong taus have an average value of 0.18±0.05, whereas 3-prong taus have a value of 0.13±0.08.

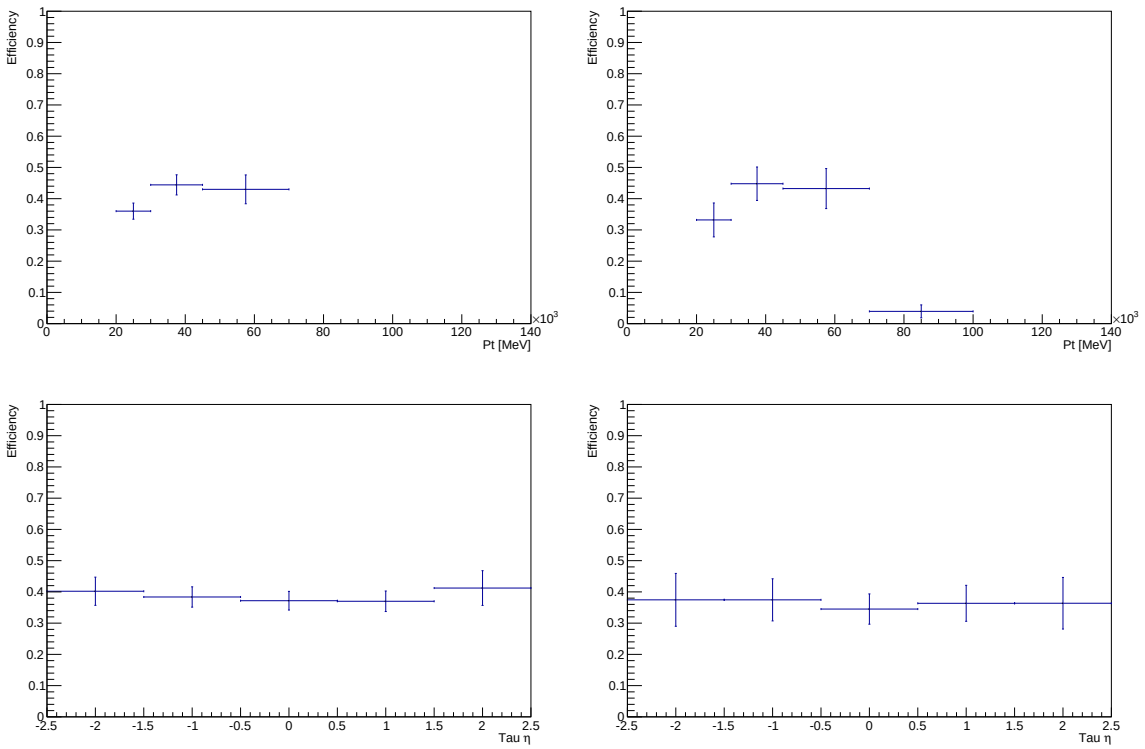

Figure 7.3: Weighted average real efficiencies of 1-prong taus (left) and 3-prong taus (right) as a function of tau p_T and η in WCR. The uncertainties are statistical.

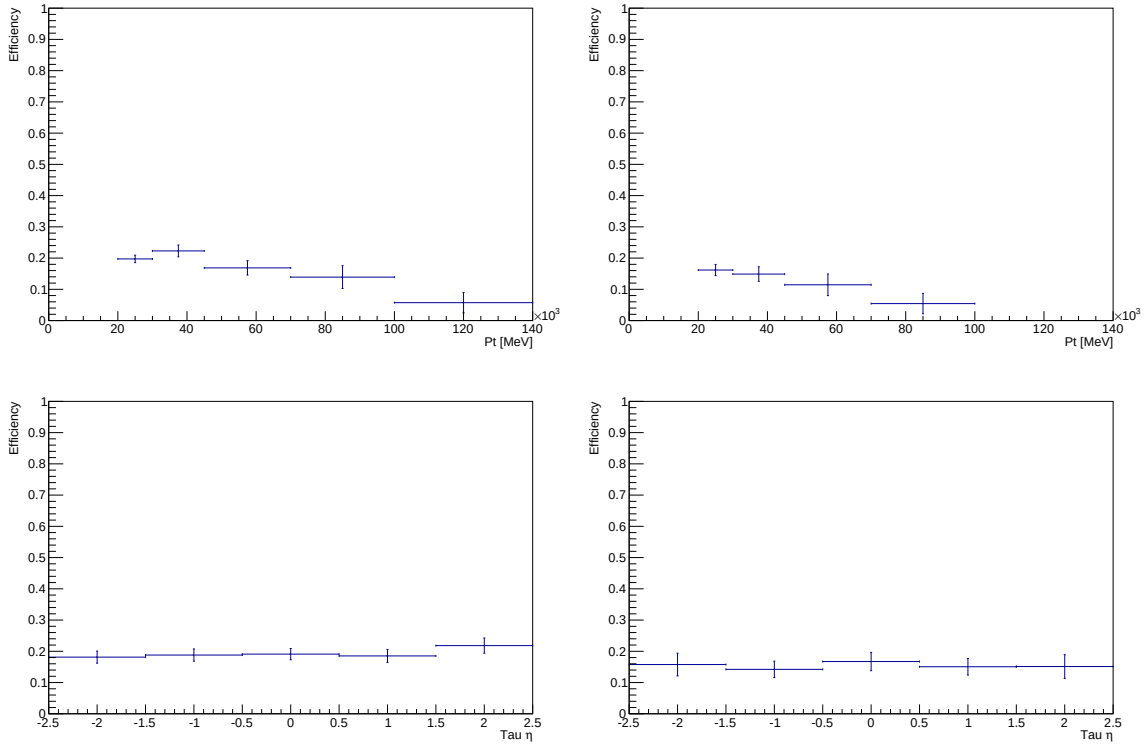

Figure 7.4: Weighted average fake efficiencies of 1-prong taus (left) and 3-prong taus (right) as a function of tau p_T and η in WCR. The uncertainties are statistical.

7.3 N^{loose} and N^{tight} Measurements

The Matrix Method is dependent on the number of events which pass the loose and tight selection criteria in the region of investigation, in this case WCR. The numbers are estimated from data measurements after subtracting the contribution of multi-jet events, in order to be consistent with the estimation of the weighted average efficiencies. The number of events in the multi-jet background is being estimated from data, as was explained in Section 6.2.1. The number of loose and tight events is defined as

$$N^{loose} = N^{loose}_{data} - N^{loose}_{multi-jet} \qquad N^{tight} = N^{tight}_{data} - N^{tight}_{multi-jet}. \tag{7.6}$$

The measurements are presented in Figure 7.5.

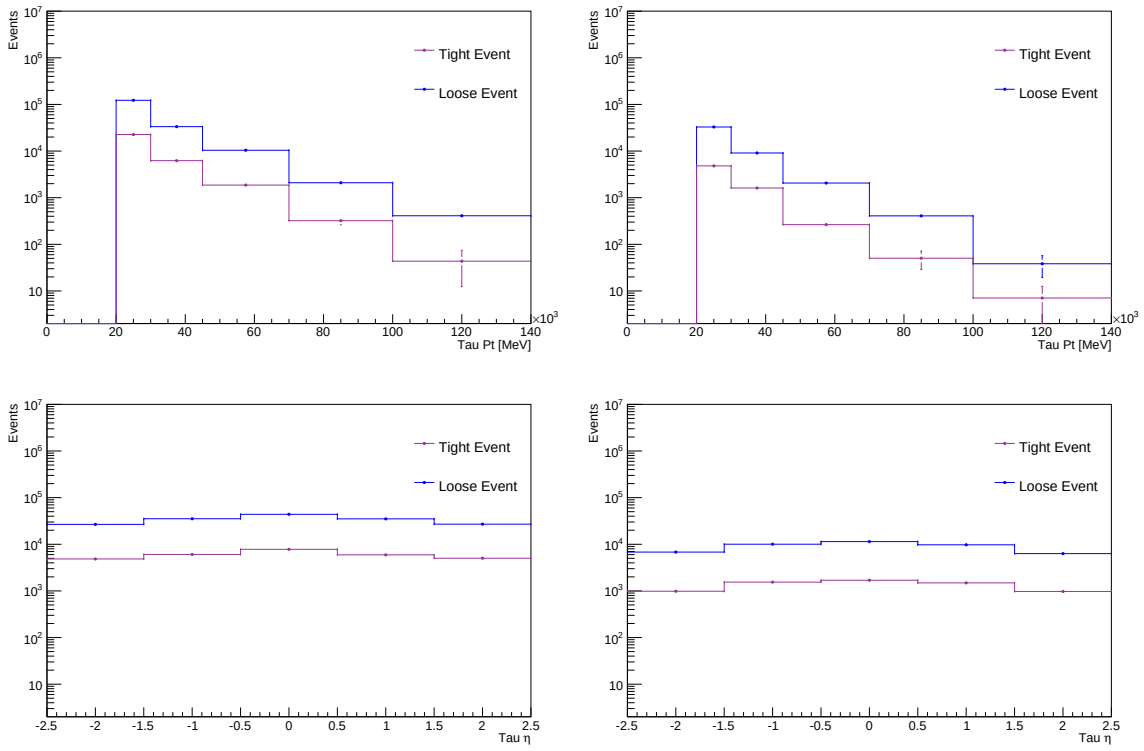

Figure 7.5: The number of loose and tight events with 1-prong taus (left) and 3-prong taus (right) as a function of tau p_T and η in WCR. The uncertainties are statistical uncertainties.

7.4 Matrix Method Results

After deriving the weighted average efficiencies and measuring the number of loose and tight events from data in WCR, we can use formula 7.3 for estimating the background in WCR.
From formula 7.3 we can indicate that the number of events with a fake tight tau is dependent on the real and fake weighted average efficiencies as well as in the number of loose and tight events. In Section 7.2 we saw that there are p_T ranges where the efficiencies have zero values. In these cases, formula 7.3 would be in the form

$$\begin{aligned} f = 0 \quad &\rightarrow \quad N_{fake}^{tight} = 0 \\ r = 0 \quad &\rightarrow \quad N_{fake}^{tight} = N^{tight}, \end{aligned}$$

namely for a fake efficiency with a zero value there is no fake background, however for a real efficiency with a zero value the fake background is maximal and includes all the tight events in the WCR.

Since the efficiencies and the number of events were parametrized by the tau p_T, η and number of prongs, the Matrix Method provides distributions for the fake background with the same dependencies.
The best way to evaluate the MM results is to sum up all contributions of the SM background with respect to their cross sections, and compare this sum with measurements from data. The SM background contributions include MC estimation

(with the truth information) for real events in W+jets, Z+jets, diboson and $t\bar{t}$ productions, multi-jet estimation from data as well as the fake background estimation from the Matrix Method.

Figure 7.6 shows the p_T distribution for 1-prong taus, split into real events from MC and fake contribution from multi-jet production and MM fake estimation in comparison with data measurements. The uncertainties are only statistical uncertainties, which are marked in red vertical lines for the total SM estimation and in black vertical lines for data.
Figure 7.7 presents a similar plot for the 3-prong taus.
In general, the agreement between data and the SM backgrounds is good with respect to the statistical uncertainties. Within the p_T ranges of 20 GeV to 30 GeV and 45 GeV to 70 GeV for 1-prong taus, as well as 30 GeV to 45 GeV for 3-prong taus, the SM estimations are not compatible with data. This estimation includes only statistical uncertainties, however the difference between data and the estimation of the SM backgrounds can be better understood when the systematic uncertainties would be taken into account.
Between the p_T range of 70 GeV to 100 GeV for 3-prong taus, the agreement between data and the SM backgrounds is very low. This is due to the small difference between the real and fake efficiencies in this range which can be seen in Figures 7.3 and 7.4. From Figure 7.7 it can be seen that between the p_T range of 100 GeV to 140 GeV there is no contribution from the fake background, this is due to the zero value of the fake efficiency (for 3-prong taus) in this range.

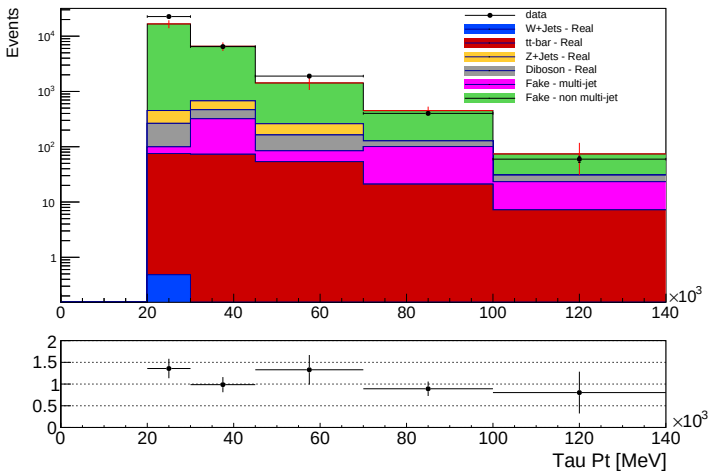

Figure 7.6: p_T distribution for 1-prong taus in real events from MC, events from multi-jet, fake estimation from the MM and data. The statistical uncertainties from the sum of MC, multi-jet and the fake background are marked by vertical red lines. The statistical uncertainties from data are marked by vertical black lines.

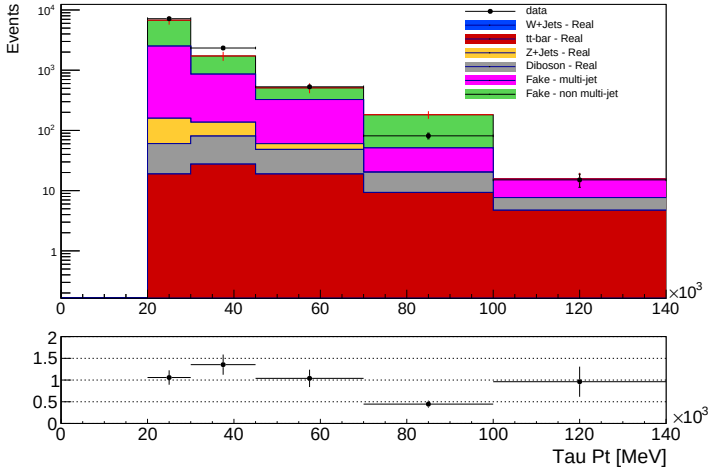

Figure 7.7: p_T distribution for 3-prong taus in real events from MC, events from multi-jet, fake estimation from the MM and data. The statistical uncertainties from the sum of MC, multi-jet and the fake background are marked by vertical red lines. The statistical uncertainties from data are marked by vertical black lines.

Figures 7.8 and 7.9 show the distributions for the tau p_T in the SM backgrounds, for events which contain real as well as fake taus. The estimation from MC for the W+jets, Z+jets, diboson and $t\bar{t}$ backgrounds is not using the truth information, i.e the events from these processes contain the fake background.
If we compare the results from the MM in Figures 7.6 and 7.7 with p_T distributions in Figures 7.8 and 7.9, we learn that the fake background is mostly dominated by W+jets production as expected to be in WCR, however there are contributions from other processes.

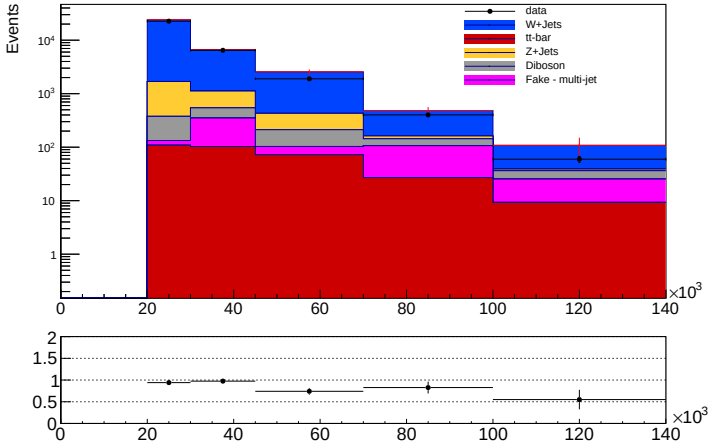

Figure 7.8: p_T distribution for 1-prong taus in the SM backgrounds (without MC truth information) and data. The statistical uncertainties from the SM backgrounds are marked by vertical red lines. The statistical uncertainties from data are marked by vertical black lines.

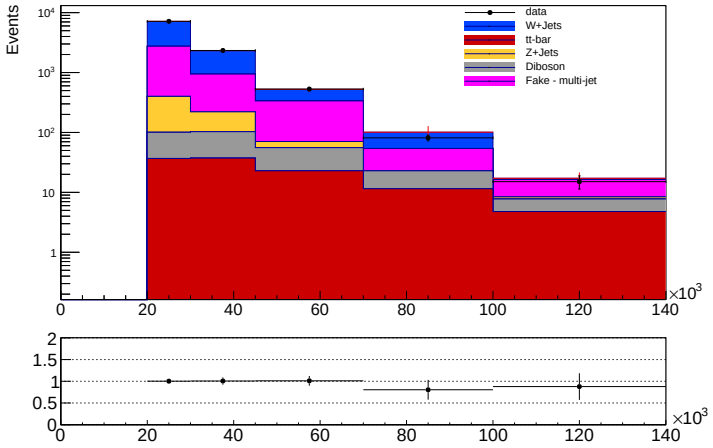

Figure 7.9: Tau p_T distribution for 3-prong tau in the SM backgrounds (without MC truth information) and data. The statistical uncertainties from SM backgrounds are marked by vertical red lines. The statistical uncertainties from data are marked by vertical black lines.

The fake background was evaluated also as a function of η. The evaluation was done in the same way as the evaluation of fake background as a function of the p_T. Figure 7.10 presents the η distribution for 1-prong taus and Figure 7.11 presents the η distribution for 3-prong taus. The agreement between data and MC is good with respect to the statistical uncertainties.

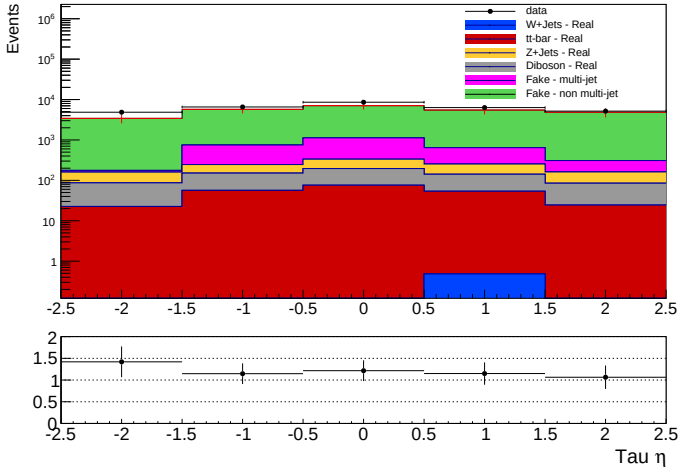

Figure 7.10: Tau η distribution for 1-prong taus in real events from MC, events from multi-jet, fake estimation and data. The statistical uncertainties from the sum of MC, multi-jet and the fake background are marked by vertical red lines. The statistical uncertainties from data are marked by vertical black lines.

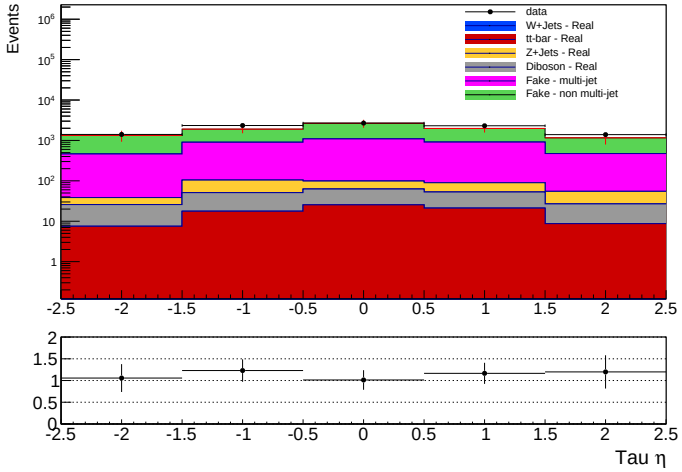

Figure 7.11: Tau η distribution for 3-prong tau in real events from MC, events from multi-jet, fake estimation and data. The statistical uncertainties from the sum of MC, multi-jet and the fake background are marked by vertical red lines. The statistical uncertainties from data are marked by vertical black lines.

7.5 Summary

In this chapter the Matrix Method for estimation of the fake background in WCR was tested.
The weighted average real and fake efficiencies, as well as the number of loose and tight events within WCR were estimated as a function of the tau p_T, η and the number of prongs in the hadronic tau decay. Between the p_T range of 70 GeV to 140 GeV, the real weighted average efficiencies has very low values with low statistics. This is cause by the real scale factors, which are measured in processes of Z bosons decays.
The average values for the efficiencies were calculated and are presented in Table 7.1.

Weighted Average Efficiency	1-prong	3-prong
Real	0.40±0.09	0.38±0.14
Fake	0.18±0.05	0.13±0.08

Table 7.1: Summary of the average values of the weighted average efficiencies

The Matrix Method yields estimation of the fake background parametrized by the tau p_T, η and the number of prongs in the decay. This estimation was combined with the estimation of the other SM backgrounds and was compared with data measurements.
In general, the agreement between data and the SM backgrounds (including the fake background) is good with respect to the statistical errors.

Chapter 8

Conclusion

This thesis is part of the ATLAS supersymmetry search with the 2012 data collected by the ATLAS experiment at a center-of-mass energy of $\sqrt{s} = 8$ TeV. It is focused on a final state with two taus and missing transverse energy after the SUSY electroweak production, when one of the tau decays hadronically and the other decays leptonically. In order to perform a precise measurement it is important to have a high accuracy prediction of the SM background. One of these backgrounds is the *fake* background. The fake background contains reconstructed leptons which originate from mis-identified objects. The aim of this analysis is to study this background.

The final state in this analysis can be detected as tau for the hadronically decaying tau and as light leptons, electron or muon, for the leptonically decaying tau. The possible origins of the leptons were estimated via the MC truth simulations for each SM production. This study shows that the reconstructed light leptons have high probability ($> 99\%$) to be real prompt leptons, whereas the taus have a probability larger than 43% to be fake. Accordingly, it was assumed to have a fake background originating only from reconstructed taus. The fake taus were found to be mostly mis-identified light flavour jets and therefore only this contribution to the fake backgrounds was taken into account in this analysis.

Two sets of selection criteria, a 'loose' and 'tight' selection, were defined with different selections of taus. The different selections enable the measurements of the real and fake efficiencies, where the real efficiency is the probability that a real loose tau is identified as a tight tau and the fake efficiency is the probability that a loose fake tau is mis-identified as a tight lepton. In order to estimate the fake background, the efficiencies were estimated from MC truth simulations and corrected for the data/MC difference via scale factors. In MC samples the estimations of the efficiencies are split into the different Standard Model backgrounds. The measurements of the efficiencies show a dependence on the number of prongs in the hadronic tau decay. The average values for the real efficiency are 0.537 ± 0.001 for 1-prong taus and 0.568 ± 0.002 for 3-prong taus. The fake efficiency has average values of 0.220 ± 0.002 for 1-prong taus and 0.157 ± 0.003 for 3-prong taus.

In order to measure the scale factors, two control regions enriched with real or fake taus (ZCR and WCR) were defined. These CRs were optimized for statistics and purity.

The real control region, ZCR, was defined to select Z+jets events, since these events contain most of the real taus. WCR is the fake control region, which was defined to

select W+jets events, which are known to contain many light flavour jets which are mis-identified as hadronic tau decays.
The scale factors between MC and data were measured in these control regions and assumed to be independent of the process, i.e the same scale factor was applied to the different SM contributions. The scale factors have a strong dependence on the parameters (p_T, η and number of prongs). The real scale factor has average values of 0.761±0.001 for 1-prong tau decays and 0.686±0.001 for 3-prong tau decays. The fake scale factor has average values of 0.937±0.005 and 0.987±0.004, respectively.

Within the estimation described above, the multi-jet production with two fake leptons was excluded since it is hard to be simulated via MC. The multi-jet production was estimated from data and was taken into account in the analysis.

The fake background can be estimated by a semi-data driven method, called the Matrix Method. This method was tested for estimation of the fake background in WCR. In order to use the matrix method it was necessary to construct the weighted average real and fake efficiencies. The weighted average efficiencies were estimated as a function of tau p_T, η and the number of prongs. The weighted average real efficiency takes into account the real efficiencies in the different SM processes, while the weighted average fake efficiency uses the fake SM efficiencies.
The weighted average real efficiency has average values of 0.40±0.09 for 1-prong taus and 0.38±0.14 for 3-prong taus. The weighted average fake efficiency has average value of 0.18±0.05 for 1-prong taus and 0.13±0.08 for 3-prong taus.
Finally, the numbers of loose and tight events in WCR were measured from data and applied together with the weighted average efficiencies to the Matrix Method. The Matrix Method provided the fake background with the same dependencies of tau p_T, η and the number of prongs. The results, namely the fake background, together with estimation of multi-jet background and the estimation of real events in MC, were compared with data measurements. The different distributions of the events as a function of the p_T and as a function of η, were shaped similarly in data and in the total estimation of the SM backgrounds, for both, 1-prong and 3-prong taus.

This study proves that the fake background can be estimated via the Matrix Method. Therefore the method is proposed for LHC run-2, which will start in 2015.

Bibliography

[1] D. Griffiths. *Introduction to Elementary Particles*. John Wiley & Sons, 1987.

[2] Perkins and Donald H. *The standard model and beyond*. CRC Press, 2010.

[3] Langacker P. *Introduction to High Energy Physics*. Cambridge Univ. Press, 2008.

[4] Stephen P. Martin. A supersymmetry primer. *JHEP*, 2011.

[5] Kazakov D.I. Gladyshev A.V. Supersymmetry and LHC. *Phys.Atom.Nucl*, 70:1553–1567, 2007. `http://arxiv.org/abs/hep-ph/0606288`.

[6] K Nakamura and Particle Data Group. Review of particle physics. *J. Phys. G: Nuclear and Particle Physics*, 37(7A):075021, 2010.

[7] The ATLAS Collaboration. A particle consistent with the higgs boson observed with the atlas detector at the large hadron collider. *Phys.Lett.*, B716(7A):30–61, 2012.

[8] The CMS Collaboration. Observation of a new boson at a mass of 125 GeV with the CMS experiment at the LHC. *Science*, 338(7A):1576–1582, 2012.

[9] Kazakov D.I. Beyond the standard model (in search of supersymmetry). *JHEP*, 2001. `http://arxiv.org/abs/hep-ph/0012288v2`.

[10] Fayet P. Farrar G.R. *Phys. Lett.*, B 76:575, 1978.

[11] `http://http://www.maayboli.com/node/3495`.

[12] Evans, Lyndon and Bryant, Philip . lhc Machine. *Jinst*, 3(S08001), 2008.

[13] `http://bigscience.web.cern.ch/bigscience/en/lhc/lhc2.html`.

[14] The ATLAS Collaboration. The ATLAS Experiment at the CERN Large Hadron Collider. *Jinst*, 3(S08003), 2008.

[15] The ATLAS Collaboration. ATLAS collaboration homepage, 2014. `http://www.atlas.ch/`.

[16] R.W.L. Jones and D. Barberis. The ATLAS computing model. *J. Phys.*, 119(072020), 2008.

[17] R.W.L. Jones and D. Barberis. The evolution of the ATLAS computing model. *J. Phys.*, 219(072037), 2010.

[18] G. Belanger, F. Boudjema, A. Cottrant, A. Pukhov, and A. Semenov. WMAP constraints on SUGRA models with non-universal gaugino masses and prospects for direct detection. *Nucl. Phys.*, B706:411–454, 2005.

[19] S.F. King, J.P. Roberts, and D.P. Roy. Natural dark matter in SUSY GUTs with non-universal gaugino masses. *JHEP*, 0710:106, 2007.

[20] The ATLAS Simulation Infrastructure. *Eur. Phys. J.*, C70:823–874, 2010. http://dx.doi.org/10.1140/epjc/s10052-010-1429-9.

[21] S. Agostinelli et al. GEANT4: A simulation toolkit. *Nucl. Instrum. Meth.*, A506:250, 2003. http://dx.doi.org/10.1016/S0168-9002(03)01368-8.

[22] Michelangelo L. Mangano, Mauro Moretti, Fulvio Piccinini, Roberto Pittau, and Antonio D. Polosa. Alpgen, a generator for hard multiparton processes in hadronic collisions. *JHEP*, 0307:001, 2003.

[23] T. Sjostrand, S. Mrenna, and P. Skands. PYTHIA 6.4 physics and manual. *JHEP*, 0605:026, 2006.

[24] T. Gleisberg et al. Event generation with sherpa 1.1. *JHEP*, 0902:007, 2009.

[25] T. Binoth, M. Ciccolini, N. Kauer, and M. Kramer. Gluon-induced W-boson pair production at the LHC. *JHEP*, 0612:046, 2006. http://dx.doi.org/10.1088/1126-6708/2006/12/046.

[26] Johan Alwall, Michel Herquet, Fabio Maltoni, Olivier Mattelaer, and Tim Stelzer. MadGraph 5 : Going Beyond. *JHEP*, 1106:128, 2011. http://dx.doi.org/10.1007/JHEP06(2011)128.

[27] S. Frixione and B. R. Webber. Matching NLO QCD computations and parton shower simulations. *JHEP*, 0206:029, 2002.

[28] S. Frixione, P. Nason, and B. R. Webber. Matching NLO QCD and parton showers in heavy flavour production. *JHEP*, 0308:007, 2003.

[29] S. Frixione, E. Laenen, P. Motylinski, and B. R. Webber. Single-top production in MC@NLO. *JHEP*, 0603:092, 2006.

[30] Borut Paul Kersevan and Elzbieta Richter-Was. The Monte Carlo event generator AcerMC versions 2.0 to 3.8 with interfaces to PYTHIA 6.4, HERWIG 6.5 and ARIADNE 4.1. *Comp. Phys. Commun.*, 184:919–985, 2013.

[31] The ATLAS Collaboration. Search for electroweak production of supersymmetric particles in final states with at least two hadronically decaying taus and missing transverse momentum with the ATLAS detector in proton-proton collisions at proton-proton collisions at $\sqrt{8}$ TeV. ATLAS-CONF-2013-028, Mar 2013.

[32] W. Lampl et al. Calorimeter clustering algorithms: Description and performance. ATL-LARG-PUB-2008-002, 2008.

[33] M. Cacciari, G. P. Salam, and G. Soyez. The anti-k_t jet clustering algorithm. *Journal of High Energy Physics*, 2008(04):063, 2008.

[34] T Barillari et al. Local hadronic calibration. Technical Report ATL-LARG-PUB-2009-001-2, CERN, Geneva, Jun 2008.

[35] The ATLAS Collaboration. Commissioning of the atlas high-performance b-tagging algorithms in the 7 tev collision data. Technical Report ATLAS-CONF-2011-102, CERN, Geneva, Jul 2011.

[36] https://twiki.cern.ch/twiki/bin/viewauth/AtlasProtected/JVFUncertaintyTool. accessible only for ATLAS users.

[37] The ATLAS Collaboration. Expected performance of the ATLAS experiment: detector, trigger and physics. *arXiv:0901.0512 [hep-ex]*, 2009.

[38] The ATLAS Collaboration. Performance of the reconstruction and identification of hadronic tau decays with atlas. Technical Report ATLAS-CONF-2011-152, CERN, Geneva, Nov 2011.

[39] The ATLAS Collaboration. Determination of the tau energy scale and the associated systematic uncertainty in proton-proton collisions at $\sqrt{s} = 7$ tev with the atlas detector at the lhc in 2011. Technical Report ATLAS-CONF-2012-054, CERN, Geneva, Jun 2012.

[40] The ATLAS Collaboration. Performance of the reconstruction and identification of hadronic tau decays in atlas with 2011 data. Technical Report ATLAS-CONF-2012-142, CERN, Geneva, October 2012.

[41] E Dawe, D O'Neil, and S Protopopescu. Using boosted decision trees for hadronic tau identification. Technical Report ATLAS-PHYS-INT-2011-004, CERN, Geneva, Jan 2011.

[42] Electron performance measurements with the ATLAS detector using the 2010 LHC proton-proton collision data. *Eur. Phys. J.*, C72:1909, 2012. `http://dx.doi.org/10.1140/epjc/s10052-012-1909-1`.

[43] The ATLAS Collaboration. Search for direct production of charginos, neutralinos and staus in final states with at least two hadronically decaying taus and missing transverse momentum in *pp* collisions at $\sqrt{8}$ TeV with the ATLAS detector. May 2014. (Not yet published).

List of Figures

Acknowledgements

First of all I want to thank to Prof. Dr. Dorothee Schaile for giving me the opportunity to expand my knowledge in the particle physics field and to be part of the great ATLAS experiment.
Many thanks to Dr. Alexander Mann and Dr. Federica Legger, my supervisors in the supersymmetry group, for the guidance and the help during this year of study.
In addition, I want to thank to Jeanette Lorenz for the advices concerning the matrix method and to Christopher Bock for the help with the code.
A Big thank to Josephine Wittkowski for helping with many different issues, professional as well as personal.
Last but not least, I want to thank to my family and friends in Israel, which supported my decision to pursue my academic studies in Germany and encouraged me during difficult times.

Declaration

I hereby declare that this thesis is my own work, and that I have not used any sources and aids other than those stated in the thesis.

München, 04.06.14

Yasmine Israeli